

AN EXAMINATION OF SUMMERTIME CYCLONE TRANSPORT PROCESSES DURING
INTEX-A

Christopher M. Kiley,¹
Henry E. Fuelberg,¹

¹Department of Meteorology, Florida State University, Tallahassee.

Submitted to

Journal of Geophysical Research
TRACE-P Special Section

January 2006

ABSTRACT

Warm conveyor belts (WCBs) are important mechanisms for transporting pollution during the cool season. These airstreams distribute surface emissions throughout the troposphere, playing a major role in the long range transport of chemical species.

Previous efforts to understand the lofting of WCBs have not investigated the relative importance of vertical forcing. In this study, we use fine resolution model-derived meteorological data, air parcel trajectories, flux calculations, and a diagnostic package for weather systems to perform a focused investigation of WCBs during the warm season INTEX-A period. Lifting and transport mechanisms during INTEX-A are compared to a well documented cool season WCB case in the literature.

Results show that weak, mid-latitude cyclones are capable of producing vertical transport as great or greater than much stronger cyclones. An analysis of forcing terms contributing to vertical motion reveals that the Laplacian of latent heat release due to convection is the primary contributor to vertical motion during some cases of INTEX-A. This convection allows weak cyclones to produce WCB-like transport.

WCB pathways are similar for the cases studied. In each example, air which originates far south of the low in the warm sector, ascends to the north, and joins the upper-level westerly flow northeast of the low center. Although the transport pathways are similar, the forcing mechanism and location of maximum vertical transport are found to exhibit strong case-to-case variability. When cyclone scale dynamics are relatively weak, widespread deep convection, especially south of the cyclone's center, is necessary to produce transport resembling a WCB.

\

1. Introduction

Understanding the mechanisms by which pollution is lofted and transported during the warm season was a major goal of NASA's Intercontinental Chemical Transport Experiment (INTEX-A) aircraft campaign [*Singh et al.*, 2006], a component of the International Consortium of Atmospheric Research on Transport and Transformation (ICARTT), that was conducted between June and August 2004. Convection and orographic flows can be important for the lifting of pollution out of the boundary layer [*Henne et al.*, 2004; *Hess*, 2005]. However, extratropical cyclones are of particular interest since their associated airstreams are thought to be the dominant mode of tropospheric trace gas transport [*Cotton et al.*, 1995; *Donnell et al.*, 2001; *Stohl*, 2001]. A greater understanding of trace gas transport from low levels to the free troposphere is needed since polluted air lifted to higher altitudes can perturb natural chemical concentrations, impact the global radiation budget, and affect the air quality at distant locations downstream.

The role of extratropical cyclones in transporting pollution across the Atlantic Ocean from the eastern United States to Europe has been the focus of several recent studies [e.g., *Bethan et al.*, 1998; *Stohl and Trickl*, 1999; *Cooper et al.*, 2001; *Stohl*, 2001; *Li et al.*, 2005] due to the potential chemical impact of the United States on European air quality and the relatively large number of aircraft campaigns that have been conducted in the region. Similarly, the role of cyclones in transporting pollution from the rapidly industrializing regions of eastern Asia to the eastern Pacific and beyond recently has gained the attention of researchers [*Hannan et al.*, 2003; *Holzer et al.*, 2003; *Cooper et al.*, 2004; *Jaffe et al.*, 2004; *Liang et al.*, 2004]. Pollution transport studies and most field campaigns primarily have focused on the cool season when transport mechanisms are thought to be most intense.

There is no thorough understanding about the role of mid-latitude cyclones and their airstreams in transporting pollution during the warm season. Such an understanding is important since mid-latitude cyclones of modest intensity represent the vast majority of all cyclone events [Roebber, 1984]. Yet the amount of research describing the life cycle and precipitation characteristics of these modest storms pales in comparison to the research on relatively rare explosively deepening cyclones [Martin, 1988]. Major mid-latitude cyclones, and their associated transport mechanisms, are cool season phenomena. Weaker mid-latitude cyclones occur during both the warm and cool seasons. Several papers have examined cyclone-related airstreams on an annual basis [e.g., Stohl, 2001; Eckhardt *et al.*, 2004] and papers by Cooper *et al.* [2001; 2004] summarized aircraft flights during the warm season. Purvis *et al.* [2003] examined convective transport in frontal regions. However, a focused investigation of transport mechanisms in warm season cyclones has not been performed.

Carlson [1980; 1988] explained that the concept of warm conveyor belts can be used to represent relative wind isentropic flow through baroclinic waves. The concept first was introduced in the late 1950's to study air motion through cumulonimbus clouds. In the middle 1960's meteorologists in the United Kingdom applied it to large-scale weather systems. This application represents the genesis of conveyor belt theory. More recently, three dimensional trajectories have been used to include the contribution of vertical motion.

The Lagrangian flow within mid-latitude cyclones is thought to consist of three major airstreams (Figure 1) [Browning and Harrold, 1969; Carlson, 1980; Browning and Mason, 1981; Carlson, 1998; Schultz, 2001]. The warm conveyor belt (WCB) is a warm moist flow that ascends from the boundary layer and lower troposphere ahead of the surface cold front. Once poleward of the surface warm front, the WCB turns anticyclonically toward the east. The cold

conveyor belt (CCB) is a weaker flow, often confined to lower levels and generally flowing from east to west in a system-relative framework on the cold side of the surface warm front. The CCB flows under the WCB and ascends anticyclonically to the northwest of the surface low pressure, similar to the WCB. Finally, the dry intrusion (DI) is a descending flow behind the surface cold front that inhibits cloud formation and is the source of the “dry slot” often seen in satellite water vapor imagery. It is clear that the airstreams are important for distributing surface emissions throughout the troposphere and in their long range transport.

Recent studies have focused on classifying airstreams and conveyor belts by imposing specific criteria on large grids of trajectories [*Wernli, 1997; Wernli and Davies, 1997; Stohl and Trickl, 1999; Stohl, 2001*]. This procedure, termed “coherent ensemble of trajectories” (CETs), isolates groups of trajectories having similar properties and/or histories. For example, *Wernli and Davies* [1997] selected the combination of strong ascent, large decreases in specific humidity, small values of potential vorticity, and large increases in potential temperature along forward trajectory paths to be indicators of warm conveyor belts. The use of CETs extended conventional WCB thinking from absolute to system-relative coordinates.

While developing a one-year climatology of northern hemispheric airstreams, *Stohl* [2001] specified criteria for WCBs based on the ascent rates of forward trajectories over a particular period of time and from certain vertical locations. Like *Wernli* [1997] and *Wernli and Davies* [1997], *Stohl* [2001] used criteria that only identified “strong” conveyor belts. Using a similar method, *Esler et al.* [2003] examined Lagrangian air mass properties across cold fronts via the reverse-domain-filling technique (RDF) [*Sutton et al., 1994*]. Their method employed trajectories that were calculated with both mesoscale and global model data.

The techniques just described take advantage of modern computing capabilities to analyze atmospheric motions with much more precision than in the past. They also eliminate the time consuming and subjective processes of manually analyzing large numbers of trajectories and/or numerous instantaneous fields at various times and altitudes. Their only significant sensitivities are the accuracy and time interval of the wind data being used. Wind data at 1-h temporal resolution have been found necessary to appropriately diagnose rapidly evolving airstreams, particularly those near the surface [*Cohen and Kreitzberg, 1997*].

The goal of this study is to quantify the vertical transport of lower tropospheric air by relatively weak mid-latitude cyclones during the warm season of INTEX-A. The characteristics and transport capabilities of several presumed WCBs during INTEX-A are examined. Ascending airstreams are identified using the coherent ensembles of trajectories (CET) technique and then are discussed in the context of the meteorological histories of trajectories through time. These INTEX-A cases are compared to a well documented cool season WCB. This research differs from previous airstream studies by concentrating on the relative importance of the vertical forcing associated with WCBs.

2. Data and Methodology

We used the Fifth-Generation National Center for Atmospheric Research/ Pennsylvania State University Mesoscale Model (MM5) to generate the hourly meteorological data needed for this study. MM5 is a nonhydrostatic, primitive equation model that is described by *Anthes and Warner [1978]*, *Dudhia [1993]*, and *Grell et al. [1994]*. Model output, rather than analyses from the global centers, was used to provide enhanced spatial and temporal resolution. In particular, hourly wind data were needed to produce reliable trajectories near cyclones [*Doty*

and Perkey, 1993]. In addition, the MM5 convective parameterization scheme provided necessary output that was not available in standard reanalysis data.

Our model domain was centered over the eastern United States and western Atlantic Ocean, and extended well beyond this region to reduce the effects of boundary error propagation into the area of interest [Warner *et al.*, 1997]. The grid for all simulations had 60 km horizontal separation and utilized 40 vertical sigma levels. The fifteen levels that were below 850 hPa had 10 hPa separation to provide enhanced vertical resolution at low altitudes. Within the middle troposphere, the vertical grid spacing was stretched to ~ 25 hPa up to an altitude of ~ 400 hPa. Above 400 hPa the grid spacing was ~ 50 hPa, with the top of the model being 100 hPa.

Model physical and dynamical parameterization schemes were identical for all simulations. We used the Medium Range Forecast (MRF) planetary boundary layer scheme [Hong and Pan, 1996], the Kain-Fritsch cumulus parameterization scheme [Kain and Fritsch, 1993], and a simple ice microphysical scheme.

Initial and lateral boundary conditions for the MM5 were obtained from three-dimensional (3-D) global reanalyses prepared by the National Center for Environmental Prediction (NCEP) [Kalnay *et al.*, 1996] and available from the National Center for Atmospheric Research (NCAR). These data were at 6 h intervals and 1.0° horizontal resolution. Two-dimensional data sets specifying sea surface temperatures also were obtained from NCEP, while land use and terrain characteristics were acquired from NCAR. Four-dimensional data assimilation (FDDA) was employed throughout the simulations to relax the model solutions toward the synoptic analyses. Although a free running model can diverge from reality, a constrained model can exhibit unphysical features arising from the model's need to balance itself against the constraint. Nonetheless, FDDA is widely used since it generally yields a better

placement of meteorological features and effectively reduces the growth of model error [*Stauffer and Seaman, 1990; Stauffer et al., 1991; Stauffer and Seaman, 1994; Seaman and Michelson, 2000*]. MM5 simulations were begun 48 h prior to a cyclone achieving maximum intensity and run for 120 h. Data from the first 12 h of the simulations were not used to allow sufficient model spin up time.

Numerous MM5-derived fields were qualitatively compared to global analyses, satellite imagery, and aircraft measured meteorological fields to verify the quality of the simulations. Close agreement was found in all cases with respect to the placement, intensity, and propagation of major meteorological features. Similarly, the magnitudes of various parameters (e.g., wind speed and direction, temperature, humidity, etc.) also showed close agreement with the global analyses and aircraft measured variables.

We used hourly wind data from MM5 to calculate forward 48 h kinematic air trajectories. Limitations of trajectories include incorrect placement of meteorological features by the input data, insufficient spatial and temporal resolution of the wind field, and numerical limitations of the calculations themselves [*Draxler, 1991; Stohl et al., 1995; Stohl and Seibert, 1998*]. Nonetheless, kinematic trajectories have been widely used in many recent chemical transport studies [*Fuelberg et al., 2000; Stohl 2001; Hannan et al., 2003*] and are considered superior to their isentropic counterparts, particularly in areas where diabatic effects are significant. A thorough comparison of the kinematic and isentropic methods, as well as a complete description of our trajectory model, can be found in the works of *Fuelberg et al. [1996, 2000]* and *Martin et al. [2002]*. Compared to earlier versions of the code, the current trajectories were not terminated if they intersected the lower boundary, but instead continued isobarically along the boundary and possibly were lofted by vertical motion at a later time, a procedure similar to *Stohl et al. [1995]*.

Another important difference is that the current advection scheme now is iterative over a 1 min interval.

Our forward trajectories were launched from four altitudes (975, 950, 925, and 900 hPa), with starting locations separated horizontally by 1.0° latitude and longitude. Trajectories were initialized over a domain stretching from 25° N to 55° N and 100° W to 50° W. Trajectory runs were made for each cyclone of interest beginning at 30, 24, and 18 h before the cyclone achieved maximum intensity. This grid of 6324 trajectories was calculated forward in time for 48 h or until they left the computational domain. Since each of the runs showed similar results, later sections only discuss trajectories launched at 900 hPa, 24 h prior to the cyclone achieving maximum intensity. Latitude, longitude, pressure height, 3-D wind components, temperature, and specific humidity were saved each hour along the trajectory paths. In addition, potential temperature, equivalent potential temperature, and relative humidity were calculated along each path and saved hourly.

We used both Lagrangian and Eulerian analyses in our study. First, the trajectory approach was employed for WCB calculations. This Lagrangian approach allows one to determine motion integrated over time, which is directly relevant to the transport of air and pollutants. Next, we used a purely Eulerian analysis to identify the role of sub-grid scale convective processes. In particular, vertical mass fluxes were calculated at a single instant in time.

3. Results

Each day during the warm season of INTEX-A was examined for vertical transport by relatively weak mid-latitude cyclones using the coherent ensemble of trajectories (CET)

technique. A total of eight WCBs were identified based on the specific criteria chosen. Two examples of typical cyclones observed during INTEX-A are presented here. These two INTEX-A examples are compared to Carlson's [1980] WCB definition established during the cool season.

3.1 Cases Selected

Carlson examined several cases of mid-latitude cyclones using isentropic analyses. He used the case study of 5 December 1977 to illustrate air motions through a typical intense mid-latitude cyclone [Carlson, 1980; 1998].

Figure 2 depicts the MM5 48 h forecast valid at 1200 UTC 5 December 1977, the time of the cyclone's maximum intensity. A surface cyclone with a central pressure of approximately 996 hPa (Figure 2b) had been intensifying rapidly during the previous 12 h and now was located over the Ohio River Valley. Deep convection was virtually absent during this case although there was widespread stable precipitation. At 500 hPa (Figure 2a), a broad planetary-scale trough was situated over the central United States. Although this cyclone was continental, climatologies have shown that most WCBs are associated with oceanic cyclones [Eckhardt *et al.*, 2004].

Wernli and Davies [1997] and *Wernli* [1997] showed that airstreams can be isolated by selecting trajectories meeting certain criteria. Suitable criteria for WCBs are a strong decrease in specific humidity, large potential temperature increases, and ascent [*Wernli and Davies*, 1997]. Threshold values of the variables used to define the airstreams are somewhat arbitrary. For example, the ascent of WCBs can range from a few thousand meters to 10,000 m or more, depending on the synoptic situation. Also the timescales over which this ascent occurs are partly arbitrary. We used a 48 h trajectory interval, because this is approximately the timescale at which

air passes through a single synoptic system. Similar to *Stohl* [2001], we initially isolated the WCBs based on ascent criteria. *Stohl* [2001] required 8000 m of ascent within 48 h, a threshold met only by strong WCBs. Therefore, we chose 5000 m over 48 h from a starting level of 900 hPa to include weaker WCBs. We used results from *Eckhardt et al.* [2003] to establish additional criteria based on specific humidity and potential temperature. In particular, after 48 h, potential temperature values must be 15 K warmer than at the starting point, and specific humidity must be 10 g kg^{-1} less than at the starting point. We employed these same criteria for both the cool and warm season cases.

Vertical transport by this cold season cyclone is revealed by the 48 h CET starting at 1200 UTC 4 December (Figure 3). The top panel shows a horizontal perspective of the CET trajectories, while the lower panel provides their pressure altitude vs. longitude. The CET on 5 December (Figure 3) agrees well with Carlson's [1980] conceptual WCB model. Specifically, warm, moist air enters the warm sector from the southwest and flows north of the warm front. After reaching saturation, the air ascends to the upper troposphere ($\sim 500 \text{ hPa}$) over New England near the ridge and then travels toward the downstream trough. Using this case, *Carlson* [1980; 1988] defined the WCB as “that air which originated far south of the low in the warm sector, ascended toward the north, achieved saturation near or north of the warm front, where it rose more rapidly, and joined the upper-level westerly flow northeast of the low center.”

Our warm season cases occurred during the INTEX-A field campaign (July – August, 2004). Figure 4a shows the 500 hPa geopotential height anomaly (1979 – 1995) for this 7 week period [*Kalnay et al.*, 1996]. The mean sea level pressure anomaly exhibits similar features over the Southeast (Figure 4b). Specifically, the reduced influence of the semi-permanent Bermuda High over the Southeast during INTEX-A permitted more frequent than typical frontal passages

through the region. The Gulf Coast often does not experience a single frontal passage during a summer season, but during INTEX-A, five fronts passed through the area. However, an examination of daily surface analyses shows that the strength of the associated cyclones was typical to slightly weaker than normal. Minimum central pressures during INTEX-A never were less than 1000 hPa. The two cases that are examined next represent typical cyclones during the INTEX-A campaign.

INTEX-A case 1 is representative of four cyclones during the campaign (18 – 19 July, 25 – 29 July, 5 – 8 August, and 13 – 14 August). Each cyclone displayed similar minimum central pressure, cyclone track, and WCB structure. Figure 5 depicts the MM5 48 h forecast valid at 0600 UTC 19 July 2004. At the surface (Figure 5b), a broad low pressure area blanketed much of the eastern seaboard. The cyclone's minimum central pressure had remained fairly steady during the previous 12 h and is now ~ 1012 hPa. At 500 hPa (Figure 5a), the flow was dominated by a closed anticyclone and ridge over the western United States and a deep trough along the Appalachians that stretches southward over the Gulf of Mexico. A closed low pressure center was located over upstate New York.

Figure 6 shows the 48 h CET depicting the vertical transport of air by the cyclone. The CET resembles the cool season case (Figure 3) with southwesterly flow ascending over time. However, the INTEX-A CET ascends higher in the atmosphere, extending above 300 hPa, compared to ~ 500 hPa for Carlson's case. This additional ascent occurs in spite of the likely weaker gradients in the large scale baroclinic environment during the summer. Weaker gradients suggest that the baroclinic terms are relatively small and that the enhanced lift must come from some other source, e.g., strong latent heat release. This hypothesis is examined in detail in later sections.

INTEX-A case 2 is representative of two cyclones during the campaign (6 – 7 July and 10 – 11 July). Both cyclones displayed similar minimum central pressure, cyclone track, and WCB structure. Figure 7 depicts the MM5 48 h forecast valid at 1800 UTC 6 July 2004. This cyclone more closely resembles the size and location of Carlson’s cool season case. At the surface (Figure 7b), a fairly compact cyclone that had been intensifying during the previous 12 h now is centered over Wisconsin. However, its minimum central pressure of 1008 hPa still is considerably greater than the 996 hPa for the cool season case. At 500 hPa (Figure 7a), a broad trough is situated over the central United States. Its amplitude is similar to that during 1977 (Figure 2a), but somewhat smaller than during INTEX-A case 1 (Figure 5a). Ridging associated with an anticyclone over the Gulf Coast extends along the East Coast. Given the characteristics of this cyclone, we thought that a CET resembling a WCB would exist. However, results (not shown) reveal that not a single trajectory met the criteria. This lack of a CET indicates that merely decreasing the central pressure of a cyclone does not necessarily result in enhanced vertical transport.

The reader is reminded that our CET criteria are somewhat arbitrary. We chose criteria to include WCBs of weaker magnitudes than examined previously [Stohl, 2001; Eckhardt *et al.*, 2003]. Although reducing the criteria even further might yield a CET, it would have much reduced vertical transport capabilities.

3.2 Grid Scale Vertical Transport

Figure 8 depicts the MM5 forecasts of 700 hPa grid scale vertical motion for each case. The 1977 cool season case (Figure 8a) exhibits a well defined area of grid scale vertical motion near the center of the cyclone, as well as a smaller area extending south along the front (Figure

2b). INTEX-A case 1 (Figure 8b) contains a stronger, but more narrow band of grid scale ascent (note the different color scale). It is important to note that the maximum grid scale vertical motion associated with the relatively weak INTEX-A case 1 cyclone is nearly 65% greater than that of the stronger 1977 case (0.14 m s^{-1} vs. 0.09 m s^{-1}). Similar to INTEX-A case 1, INTEX-A case 2 (Figure 8c) also exhibits a narrow band of grid scale vertical motion. However, the magnitude of INTEX-A case 2 grid scale vertical motion is rather weak, and no WCB-like CET is produced.

Figure 9 shows plots of trajectory heights vs. time for the two CETs. Strong vertical ascent is associated with both the cool and warm season CETs, with a mean slope of $12.28 \text{ (hPa h}^{-1}\text{)}$ for Carlson's case (Figure 9a) and $13.34 \text{ (hPa h}^{-1}\text{)}$ for INTEX-A case 1 (Figure 9b). INTEX-A case 1 exhibits fairly constant ascent throughout the entire 48 h period reaching 700 hPa in 12 h. Carlson's 1977 case shows the strongest ascent centered around $t=24 \text{ h}$, the time of maximum cyclone intensity.

To quantify the magnitude of grid scale vertical transport through each CET, upward mass flux (UMF) was calculated in three different areas around the center of each cyclone. UMF (kg s^{-1}) is simply the mass of air passing through a certain level over time. It was calculated using the grid scale vertical motions for each trajectory (i) comprising the CET, that is

$$UMF = \sum_i \frac{\omega_i \times area}{g} \quad (1)$$

where ω_i is vertical motion expressed in units of force per unit area per unit time ($\text{kg m s}^{-2} \text{ m}^{-2} \text{ s}^{-1}$), area is the MM5 60 km horizontal resolution squared (m^2), and g is the acceleration of gravity (m s^{-2}). The total UMF for each CET is reported, i.e., total UMF is the sum of UMF calculations for each trajectory comprising the CET.

UMF calculations are presented for the two CETs meeting the criteria described earlier (Carlson's case and INTEX-A case 1). Figure 10 shows the three $10^\circ \times 10^\circ$ study areas used for each cyclone superimposed on the MM5 forecast of 700 hPa streamlines. Since the cyclones are approximately vertically stacked, the 700 hPa streamlines are similar to those at other levels.

Box 1 boundaries in the x-direction were defined as the cyclone center and 10° east of the center, while in the y-direction they stretched from 5° south of the cyclone to 5° north. This position is consistent with the CET plots which show most trajectories passing through this region. The position also agrees with Carlson's WCB definition which indicates that parcels should experience their greatest ascent in this area while passing over the warm front. Box 2 was shifted 10° south of Box 1, and Box 3 was shifted 10° west of Box 2. One should note that Box 2 of the INTEX-A case mostly is located over water, while Carlson's Box 2 is more continental. CETs within each box were used to calculate UMF.

Table 1a shows UMF calculations in Box 1 at four levels (850, 700, 500, and 300 hPa) for the two cyclones having a WCB-like CET. Magnitudes of UMF are similar for both cases in the lowest level (850 hPa) east of the cyclone. Results for Carlson's 1977 case at 850 hPa are an order of magnitude smaller than those calculated by *Eckhardt et al.* [2003] for a cool season WCB ($3.7 \times 10^8 \text{ kg s}^{-1}$ vs. $7.7 \times 10^9 \text{ kg s}^{-1}$).

UMFs in Box 1 at mid levels (700 and 500 hPa) are much stronger for Carlson's case than the warm season INTEX-A case. However, the strength of the INTEX-A warm season UMF in the upper levels (300 hPa) is greater than during Carlson's cool season case. As noted previously, enhanced latent heat release in the potentially weaker gradients of the large scale baroclinic environment during summer could provide the additional lift needed for the warm season CET to extend above 300 hPa (discussed further in Section 3.5).

The northerly ascent of the CETs (Figures 3 and 6) suggests that we examine UMF in regions south and west of the cyclone's center. Table 1b contains the Box 2 UMF calculations for the CETs in the Carlson and INTEX-A cases. Carlson's cool season results exhibit vertical transport through the lower levels (850 and 700 hPa), but none in the upper troposphere. This gradual ascent from the south at low levels (Box 2) continues towards the warm front (Box 1) where the air ascends more rapidly and is transported to the upper levels, consistent with Carlson's WCB model. The INTEX-A values show a different result. Shifting the box 10° south (Box 2) produces much stronger UMF at all levels. These large magnitudes farther south are greater than those of the cool season case directly east of the cyclone center (Box 1).

Table 1c shows UMF southwest of the 700 hPa cyclone center (Box 3). The cool season results continue to support Carlson's WCB definition, with ascent only at low levels from the south. Conversely, the warm season INTEX-A results again show strong UMF in the lower and middle troposphere. Magnitudes in warm season Box 3 are stronger than those through Box 1, but weaker than those through Box 2. In summary, Carlson's cool season UMF is greatest east of the cyclone's center (Box 1), although intense vertical transport has been documented in other areas of wintertime cyclones (e.g., *Wernli [1997]*). The warm season INTEX-A UMF is strongest south and southwest of the cyclone (Boxes 2 and 3). Nonetheless, it is clear that both CETs are associated with major upward transport that can alter the atmospheric chemistry of the upper troposphere.

Current findings agree with *Carlson [1998]* who noted that the instantaneous vertical motion and vertical displacement of WCB air depend on the initial moisture content at the WCB's source and the mid-level temperature near the trajectory terminus. Where the WCB air exhibits a large specific humidity, the conveyor belt is latitudinally and vertically extensive. The

INTEX-A case 1 WCB air ascends higher than in Carlson's case and the INTEX-A case does indeed have a greater specific humidity in the lower levels. Specifically, the INTEX-A case 1 mean specific humidity from the surface to 850 hPa near the CET's source is $0.013 \text{ (kg kg}^{-1}\text{)}$, while the specific humidity in Carlson's case is only $0.003 \text{ (kg kg}^{-1}\text{)}$. Thus, the CET having the greatest moisture content also exhibits the greatest ascent.

3.3 Sub-Grid Scale Vertical Transport

WCBs often are defined from satellite imagery alone [e.g., *Carlson, 1998; Cooper et al., 2003; Li et al., 2005*]. Typically, a broad area of clouds extends north of the warm front, and a narrower zone of clouds trails southward along the cold front, as illustrated by the GOES-12 image for INTEX-A case 1 (Figure 11) 12 h after the trajectories were started. This southward extension of clouds usually is assumed to represent the WCB. The role of convection that often is embedded within these cloud systems is examined next.

Since our MM5 simulations were run at 60 km horizontal resolution, the convection was sub-grid scale and was required to be parameterized. Unlike actual convection, convective parameterization schemes (CPS) do not directly change the larger scale winds, nor do they directly affect the grid scale vertical motion. However, the winds can change in response to the warming created by the latent heat release of an active CPS. Specifically, the heating and moisture modifications induced by a CPS produce changes to the height field and, in turn, the winds. The impact of an active CPS on the wind field depends on the size of the convective area. However, *Fuelberg and Printy [1983]* used radiosonde data to show that sub-synoptic scale deep convection can affect environmental winds within 1-3 h of storm initiation.

The parameterized convective rainfall total is a standard output parameter from MM5 and many other atmospheric models. *Kain et al. [2003]* noted, "it is unfortunate that operational

models provide only this single measure of convective intensity because accumulated precipitation is a superficial and often ambiguous reflection of the vigor of convection.” For example, some severe thunderstorms produce minimal rainfall, such as low-precipitation supercells [Bluestein and Parks, 1983] or convection associated with dry microbursts [Wakimoto, 1985]. Thus, precipitation amounts do not necessarily correspond to the intensity of convection.

The *Kain-Fritsch* [1993, 2003] CPS used in our study was modified to obtain information on the vertical distribution of convective scale transport. Values of non-normalized convective scale mass flux (CMF) (kg s^{-1}) were calculated using (1), but with omega equal to the sub-grid scale vertical motion from the CPS. Total CMF for each CET is reported, i.e., CMF is the sum of sub-grid scale CMF calculations for each trajectory comprising the CET. This allows the direct comparison between grid scale UMF (Table 1) and sub-grid scale CMF. CMF was calculated at model levels throughout the troposphere.

Table 2 shows CMF for INTEX-A case 1. Since CMF was found to be zero along the CET east of the cyclone (Figure 10b, Box 1), it is not included in Table 2. Although low altitude convection was noted east of the cyclone (Figure 10b, Box 1), the altitude of the case 1 CET in this region (Figure 6) is higher than 500 hPa. Thus, CMF is zero because the CET in that region is located above the convection. However, CMF does influence areas south (Figure 10b, Box 2) and southwest (Figure 10b, Box 3) of the cyclone. Specifically, greatest magnitudes of CMF mostly are located southwest (Figure 10b, Box 3) of the cyclone center in association with frontal and sea breeze induced deep convection along the Gulf Coast (e.g., Figure 11). South of the INTEX-A case 1 cyclone (Figure 10b, Box 2), convection is important at all levels. In particular, CMF dominates the advective flux at 300 hPa. However, in the southwest region

(Figure 10b, Box 3), the tables indicate that convection is the dominant lofting mechanism in the mid levels (700 and 500 hPa) and important at all levels of INTEX-A case 1.

Unlike INTEX-A case 1, CMF in Carlson's CET is zero within all three study areas (Figure 10a). Nonetheless, shallow convection is present southwest of the cool season cyclone, and the CET passes through this region at low levels (Figure 3). Therefore, one expects the CET in this area to be influenced by CMF (Figure 10a, Box 3). Additional analyses explain this apparent contradiction. Specifically, CMF influences Carlson's CET only at very low levels ($p > 880$ hPa) southwest of the cyclone (Figure 10a, Box 3). However, since our calculations only consider transport through 850 hPa and above (Tables 1 and 2), the influence of convection at even lower levels is not identified. For example, when grid scale UMF and sub-grid scale CMF were calculated at 880 hPa southwest of the cyclone (Figure 10a, Box 3), grid-scale UMF ($38.6 \times 10^7 \text{ kg s}^{-1}$) is much larger than sub-grid scale CMF ($11.7 \times 10^7 \text{ kg s}^{-1}$). These findings suggest that vertical motion forcing due to latent heat release is much smaller than due to differential absolute vorticity advection at most levels within Carlson's CET. Vertical transport mechanisms for the two warm season INTEX-A cases will be examined in the next section.

Although convection does not influence the 1977 CET except at the very lowest levels, convection does influence some cool season WCB-like CETs at higher levels. For example, we modeled a cyclone on 9 February 2001, and the results revealed a CET meeting the criteria used in Carlson's case. Although, this CET was influenced by CMF at upper levels, values were less than $25 \times 10^7 \text{ kg s}^{-1}$, compared to grid scale UMF of $\sim 40 \times 10^7 \text{ kg s}^{-1}$. This suggests that convection supported vertical motion within the CET; however, forcing by larger scale processes (e.g., differential absolute vorticity advection and the Laplacian of temperature advection) also were major contributors to vertical motion. In general, the convective influence

on these two cool season cases was found to be weaker than during the INTEX-A warm season cases.

Finally, one should recall that INTEX-A case 2 did not include a WCB-like CET. Thus, values of CMF for Table 2 could not be computed.

In summary, an important hypothesis at this point (Figure 12b and Table 2) is that convectively induced latent heat release is the dominant cause of enhanced vertical motion during the warm season INTEX-A case 1. And, unlike Carlson's case, this enhanced vertical motion is located several hundred kilometers away from the center of the cyclone (Figure 7b) along the southern extent of the cold front.

3.4 Contributions to Vertical Transport

Although the previous section hypothesized that convection provided a major influence on vertical motion during INTEX-A case 1, we have not yet quantified the magnitude of the convective contribution. Therefore, we next use a diagnostic package for weather systems called DIONYSOS [*Caron et al.*, 2005] to compute contributions to vertical motion by an extensive set of dynamical and thermodynamical forcing terms, including vorticity and temperature advection, latent and sensible heating, friction, and orography. DIONYSOS utilizes the complete hydrostatic omega equation in pressure coordinates [*Raisanen*, 1995]:

$$\begin{aligned}
 & \frac{R}{p} \nabla^2 S\omega + f(f + \zeta) \frac{\partial^2 \omega}{\partial p^2} - f\omega \frac{\partial^2 \zeta}{\partial p^2} - f \frac{\partial}{\partial p} \left(\frac{\partial \omega}{\partial x} \frac{\partial v}{\partial p} - \frac{\partial \omega}{\partial y} \frac{\partial u}{\partial p} \right) \\
 & = \underbrace{-\frac{R}{p} \nabla^2 (-V \cdot \nabla T)}_{\text{LTA}} - \underbrace{\frac{R}{p} \nabla^2 \frac{q}{c_p}}_{\text{LDH}} - f \frac{\partial}{\partial p} \underbrace{[-V \cdot \nabla (f + \zeta)]}_{\text{VA}}
 \end{aligned} \tag{3}$$

$$-f \frac{\partial}{\partial p} (k \cdot \nabla \times F) + f \frac{\partial}{\partial p} \left(\frac{\partial \zeta_{AG}}{\partial t} \right)$$

FR **AG**

Each of the symbols has its usual meteorological meaning [e.g., *Holton* 1992, pp. 476-479] except for F which represents frictional forcing. On the right side, the six forcing terms represent the Laplacian of temperature advection (LTA) and the Laplacian of diabatic heating (LDH) which, in DIONYSOS, consists only of sensible heat flux (LSH) and latent heat release (LLH) terms. The right side also includes terms for differential vorticity advection (VA), friction (FR), and ageostrophic vorticity tendency (AG). The AG term is neglected. Since the left side of (3) is linear with respect to omega, the contributions of the five dependent forcing terms to vertical motion can be calculated separately by imposing homogenous conditions ($\omega = 0$) on all boundaries (lateral, upper, and lower). Orographic effects (OR) are computed by imposing a diagnosed surface vertical motion (obtained from horizontal winds and topography) as the lower boundary condition in (3) and then solving the equation with all forcing terms and the vertical motion at the upper and lateral boundaries set to zero.

One should note that to quantify magnitudes of the different vertical forcing terms we use both non-hydrostatic and hydrostatic approaches. In particular, DIONYSOS assumes hydrostatic conditions. However, the non-hydrostatic MM5 model was used to calculate our Lagrangian trajectory calculations and mass flux estimates.

DIONYSOS was run at 6 hourly intervals on both INTEX-A cases for 48 h periods centered on the time of each cyclone achieving maximum intensity. Since the relative contributions of forcing terms remained consistent during their respective 48 h periods, only

results at the time of maximum cyclone intensity are presented. Figure 12 shows results at 500 hPa for INTEX-A case 1. The location of the CET (Figure 6) is evident in the total vertical motion forcing field (Figure 12g). Figure 12d identifies the Laplacian of latent heat release as the primary contributor to vertical motion at 500 hPa. This term is greatest in areas of deep convection (Figure 12b). Figure 13a is a vertical profile through the region of maximum upward motion east of the Mid-Atlantic states (38° N, 68° W) (Figure 12g), while Figure 13b is a profile through the region of enhanced ascent south of the Gulf Coast (28° N, 86° W) (Figure 12g). Both profiles document that the Laplacian of latent heat release is the dominant contributor to vertical motion at all levels of INTEX-A case 1, with greatest values in the middle troposphere. This finding contrasts with many cyclones where the differential absolute vorticity advection and Laplacian of temperature advection terms often are the two greatest contributors to vertical motion [Pinot *et al.*, 1992; Bluestein, 1993].

Results for INTEX-A case 2 are shown in Figure 14. The region of maximum vertical motion forcing near Lake Superior (49° N, 96° W) (Figure 14g) is associated with our cyclone of interest. Several terms provide important contributions to ascending motion (Figure 15); however, differential absolute vorticity advection provides the greatest overall contribution. Friction is the greatest contributor in the lowest levels, while the Laplacian of temperature advection contributes significantly throughout the profile. No single term dominates the vertical motion forcing during Case 2. This finding contrasts with INTEX-A case 1 where the latent heating term clearly dominated the total vertical motion forcing.

DIONYSOS reveals that magnitudes of total vertical motion forcing near the center of each cyclone are similar for the two INTEX-A cases (Figures 12g and 14g). However, unlike INTEX-A case 2, the area of large vertical motion forcing for INTEX-A case 1 extends

southward along the front to the Gulf of Mexico. As noted earlier, this is a region of humidities. This southward extension of enhanced vertical motion appears to be critical for producing a CET meeting our criteria (Figure 6). Convection, through the Laplacian of latent heat, is the greatest contributor to vertical motion forcing in this region away from the cyclone. Thus, convection appears necessary for weak, warm season cyclones to produce a CET resembling a WCB. This result is consistent with the documentation that WCBs can exist during the early phase of cyclone development where there is almost no signature in the pressure field [*Wernli, 1997*] and that an intense dry cyclone only produces very weak ascent [*Schaer and Wernli, 1993*]. Although latent heating due to intense stable precipitation could produce a similar result, the large values of CMF indicate that convection was the dominant factor during this warm season INTEX-A event.

We were unable to run DIONYSOS on Carlson's 1977 case. However, the size and location of Carlson's cyclone (Figure 2) closely resemble that of INTEX-A case 2 (Figure 7). And, magnitudes of vertical motion for these two cases are similar (Figure 8a and c), both having a much smaller magnitude than INTEX-A case 1 (Figure 8b). Furthermore, both cases contained very little deep convection, due partly at least to their more continental character. Thus, we believe that if DIONYSOS could be run on Carlson's case, the results would be similar to INTEX-A case 2. It should be noted that we could have chosen a winter cyclone exhibiting deep convection or one with greater upward transport than the widely studied Carlson case examined here.

3.5 Role of Convection

Although we have examined only two cases in detail, we believe that results from the INTEX-A period are typical of many warm season cases when non-convective dynamics are

relatively weak. We next consider five typical warm season synoptic patterns (Figure 16) to gain a broader perspective. The first scenario (Figure 16a), similar to INTEX-A case 2, depicts a weak warm season cyclone whose cold front remains well north of the Gulf Coast in a region of only scattered convection. A WCB-like CET does not occur during this INTEX-A case, and likely does not occur in similar situations.

The second scenario (Figure 16b) contains a cold front which remains well north of the Gulf Coast but is associated with a region of widespread deep convection. This scenario was observed on 9 July near St. Louis, MO. Although somewhat similar to the 1977 cool season case (Figure 12a), this deep convection is confined to near the surface cyclone. Model derived calculations (not shown) reveal that a WCB-like CET does not result from this scenario, apparently due to the lack of convectively induced vertical transport south of the cyclone. This implies that for a weak warm season cyclone to produce a CET based on our criteria, deep convection not only must be present, but must extend south of the cyclone along the cold front. However, if this convective support is located farther south, this second scenario might produce a WCB-like feature.

The third scenario (Figure 16c) does not involve either a cyclone or front. Rather, there is interaction between widespread deep convection along the Gulf Coast and the semi-permanent Bermuda High. This interaction involves air parcels being lofted by extensive afternoon convection over the Southeast and then transported in southerly flow wrapping around the Bermuda High, thereby creating a WCB-like CET. Since there is no nearby frontal system, the convection is triggered by the sea breeze, by other mesoscale phenomena, or by westward moving easterly waves. Climatologically, this is a common scenario that appears capable of producing a WCB-like CET during stagnant conditions with a typical Bermuda High. However,

the relatively weak Bermuda High over the Southeast during INTEX-A (Figure 4), together with frequent frontal passages through the region, prevented this scenario from occurring during the study period.

The fourth scenario (Figure 16d) involves a cold front stretching to the Gulf Coast, but with minimal convection in the region. This scenario also was not identified during INTEX-A. It is believed to be uncommon during the warm season because fronts that reach the Gulf Coast during this half of the year generally trigger widespread convection. Factors such as cyclone strength and interaction with the Bermuda High will determine whether this scenario can produce a CET resembling a WCB. Finally, the fifth example (Figure 16e) depicts a front with deep convection along the Gulf Coast. INTEX-A Case 1 is typical of this scenario which results in a WCB-like feature that transports air out of the boundary layer and lower troposphere.

These five scenarios by which convection is thought to affect vertical transport are based on a similar hypothesis. Specifically, when cyclone scale dynamics are relatively weak, widespread convection is necessary to produce a CET resembling a WCB. Without widespread convection, especially south of the cyclone along the cold front, relatively weak warm season cyclones lose a necessary source for the vertical transport that is required for WCB-like airstreams.

4. Conclusions

The major objective of this study was to document the various modes of vertical transport during the warm season. Each day during the 7 week INTEX-A mission (June – August 2004) was examined for vertical transport by relatively weak mid-latitude cyclones. Two examples of typical cyclones observed during INTEX-A were presented. Ascending airstreams, i.e., possible

WCBs, were identified using the coherent ensemble of trajectories (CET) technique. The CETs were defined as having ascent of at least 5000 m over 48 h from a starting level of 900 hPa. Additional CET criteria required the potential temperature to increase by 15 K and specific humidity to decrease by 10 g kg^{-1} within 48 h. These two INTEX-A examples were compared to Carlson's well documented WCB during the cool season of 1977.

The MM5 numerical model was used to provide data at enhanced spatial and temporal resolution. In particular, hourly wind data were needed for trajectory calculations. In addition, the MM5 convective parameterization scheme provided output not available in standard reanalysis data.

The three cases modeled in this study were distinctively different from each other. The first case [Carlson, 1980] contained a major cool season continental surface cyclone. Carlson did not use trajectory analysis in his study; however, we identified a CET agreeing closely with his conceptual WCB model. Specifically, warm, moist air entered the warm sector from the south and flowed north of the warm front. After reaching saturation, the air ascended to the upper troposphere and joined the upper-level westerly flow northeast of the low center. INTEX-A case 1 involved a broad area of weak low pressure stretching over much of the eastern seaboard. This much weaker cyclone also contained a CET resembling the cool season case. The CET ascended higher in the atmosphere, extending above 300 hPa, compared to ~ 500 hPa for Carlson's CET. The low level humidity at the beginning of this CET was much greater than during Carlson's case. Finally, INTEX-A case 2 contained a rather small cyclone over Wisconsin. Although this cyclone was stronger than INTEX-A case 1, it did not produce a CET. This indicates that merely increasing the strength of a surface cyclone does not necessarily produce enhanced vertical motion.

This study has documented important characteristics of vertical transport during INTEX-A. Weak, warm season mid-latitude cyclones have been shown to be capable of producing vertical transport as great or greater than much stronger cyclones. Vertical transport through a warm season cyclone was found to be greatest away from the cyclone along the cold front. An analysis of forcing terms contributing to vertical transport revealed that the Laplacian of latent heat release term due to widespread deep convection was the primary contributor to vertical motion during the warm season INTEX-A case 1 CET. In spite of their different causes, both CETs examined in this study exhibited similar transport pathways, with each CET transporting air which originated far south of the low in the warm sector, ascending to the north, and joining the upper-level westerly flow northeast of the low center.

These results suggest that the location and support for maximum WCB vertical transport exhibit strong case-to-case variability. This variation primarily depends on whether baroclinic processes which control vorticity and temperature advection or convective dynamics are dominant. Specifically, when cyclone scale dynamics are relatively weak, widespread deep convection is necessary to produce a CET resembling a WCB. Without widespread convection, especially south of the cyclone along the cold front, relatively weak warm season cyclones lose a necessary source for the vertical transport that is required for WCB-like airstreams.

Acknowledgements. The authors would like to thank Christian Page for his help with the DIONYSIS runs.

REFERENCES

- Anthes, R. A., and T. T. Warner, Development of hydrodynamic models suitable for air pollution and other mesometeorological studies, *Mon. Wea. Rev.*, **106**, 1045-1078, 1978.
- Bader, M.J., G.S. Forbes, J.R. Grant, R.B.E. Lilley, and A.J. Waters (Eds.), A practical Guide for Interpreting Satellite and Radar Imagery, Cambridge Univ. Press, New York, 1995.
- Bethan, S., G. Vaughan, C. Gerbig, A. Volz-Thomas, H. Richer, and D. A. Tiddeman, Chemical air mass differences near fronts, *J. Geophys. Res.*, **103**, 13,413 – 13,434, 1998.
- Bluestein, H. B., *Synoptic-Dynamic Meteorology in Midlatitudes*, Vol II, Oxford University Press, 594 pp., 1993.
- Bluestein, H. B., and C. R. Parks, A synoptic and photographic climatology of low-precipitation severe thunderstorms in the southern plains, *Mon. Wea. Rev.*, **111**, 2034-2046, 1983.
- Browning, K. A., and T. W. Harrold, Air motions and precipitation growth in a wave depression, *Quart. J. Roy. Meteor. Soc.*, **95**, 288-309, 1969.
- Browning, K. A., and J. Mason, Air motion and precipitation growth in frontal systems, *PAGEOPH*, **119**, 577-593, 1981.
- Carlson, T. N., *Mid-Latitude Weather Systems*, American Meteorological Society, Boston, 1998.
- Carlson, T. N., Airflow through midlatitude cyclones and the comma cloud pattern, *Mon. Wea. Rev.*, **108**, 1498-1509, 1980.
- Caron, J. -F., P. Zwack, C. Page, A diagnostic study of the GEM operational forecast of the European windstorm 'Lothar'. Part 1: The diagnostic tool, Submitted to *Mon. Wea. Rev.*, 2005.
- Cohen, R. A., and C. W. Kreitzberg, Airstream boundaries in numerical weather simulations, *Mon. Wea. Rev.*, **125**, 168-183, 1997.
- Cooper, O. R., C. Forster, D. Parrish, M. Trainer, E. Dunlea, T. Ryerson, G. Hubler, F. Fehsenfeld, D. Nicks, J. Holloway, J. de Gouw, C. Warneke, J. M. Roberts, F. Flocke, and J. Moody, A case study of transpacific warm conveyor belt transport: In fluence of merging airstreams on trace gas import to North America *J. Geophys. Res.*, **109**(D23S08), doi:10.1029/2003JD003624, 2004.
- Cooper, O. R., J. L. Moody, D. D. Parrish, M. Trainer, T. B. Ryerson, J. S. Holloway, G. Hubler, F. C. Fehsenfeld, S. J. Oltmans, and M J. Evans, Trace gas signatures of the airstreams within North Atlantic cyclones: Case studies from the North American Regional Experiment (NARE '97) aircraft intensive, *J. Geophys. Res.*, **106**, 5437-5456, 2001.

- Cotton, W. R., G. D. Alexander, R. Hertenstein, R. L. Walko, R. L. McAnelly, and M. Nicholls, Cloud venting-A review and some new global annual estimates, *Earth Sci. Rev.*, **39**, 169-206, 1995.
- Donnell, E. A., D. J. Fish, E. M. Dicks, and A. J. Thorpe, Mechanisms for pollutant transport between the boundary layer and the free troposphere, *J. Geophys. Res.*, **106**, 7847-7856, 2001.
- Doty, K. G., and D. J. Perkey, Sensitivity of trajectory calculations to the temporal frequency of wind data, *Mon. Wea. Rev.*, **121**, 387-401, 1993.
- Draxler, R. R., The accuracy of trajectories during ANATEX calculations using dynamic model analyses versus rawinsonde observations, *J. Appl. Meteor.*, **30**, 1446-1467, 1991.
- Dudhia, J., A nonhydrostatic version of the Penn State/NCAR mesoscale model: Validation tests and simulation of an Atlantic cyclone and cold front, *Mon. Wea. Rev.*, **121**, 1493-1513, 1993.
- Eckhardt, S., A. Stohl, H. Wernli, P. James, C. Forster and N. Spichtinger, A 15-Year Climatology of Warm Conveyor Belts, *J. of Climate*, **17**, 218-237, 2004.
- Esler, J. G., and P. H. Haynes, Transport and mixing between airmasses in cold frontal regions during Dynamics and Chemistry of Frontal Zones (DCFZ), *J. Geophys. Res.*, **108**(D4), 4142, doi:10.1029/2001JD001494, 2003.
- Fuelberg, H. E., J. R. Hannan, P. F. J. van Velthoven, E. V. Browell, G. Bieberbach Jr., R. D. Knabb, G. L. Gregory, K. E. Pickering, and H. B. Selkirk, A meteorological overview of the SONEX period. *J. Geophys. Res.*, **105**, 3633-3651, 2000.
- Fuelberg, H. E., R. O. Loring Jr., M. V. Watson, M. C. Sinha, K. E. Pickering, A. M. Thompson, G. W. Sachse, D. R. Blake, and M. R. Schoelberl, TRACE-A – A trajectory intercomparison: Part 2. Isentropic and kinematic methods. *J. Geophys. Res.*, **101**, 23927-23939, 1996.
- Fuelberg, H. E., M. F. Printy, Meso beta-scale thunderstorm/environment interactions during AVE-SESAME V (20-21 May 1979), *Bull. Amer. Meteor. Soc.*, **64**, 1144-1156, 1983.
- Grell, G. A., J. Dudhia, and D. R. Stauffer, A description of the fifth-generation Penn State/MCAR mesoscale model (MM5), *NCAR Technical Note*, NCAR/TN-398+STR, 117 pp., 1994.
- Hannan, J. R., H. E. Fuelberg, J. H. Crawford, G. W. Sachse, and D. R. Blake, Role of wave cyclones in transporting boundary layer air to the free troposphere during the spring 2001 NASA/TRACE-P experiment, *J. Geophys. Res.*, **108**(D20), 8785, doi:10.1029/2002JD003105, 2003.

- Henne, S., M. Furger, S. Nyeki, M. Steinbacher, B. Neininger, S. F. J. de Wekker, J. Dommen, N. Spichtinger, A. Stohl, and A. S. H. Prevot, A quantification of topographic venting of boundary layer to the free troposphere, *Atmos. Chem. Phys.*, **4**, 497-509, 2004.
- Hess, P. G., A comparison of two paradigms: The relative global roles of moist convective versus nonconvective transport, *J. Geophys. Res.*, **110**, D20302, doi:10.1029/2004JD005456, 2004.
- Holton, J. R., *An introduction to dynamic meteorology*, 3d ed. Academic Press, 511 pp., 1992.
- Holzer, M., I. G. Mc Kendry, and D.A Jaffe, Springtime Trans-Pacific atmospheric transport from East Asia: A transit-time-PDF approach, *J. Geophys Res.*, Vol. **108**, No. D22, 4708, 10.1029/2003JD003558, 2003.
- Hong, S.-Y., and K.-L Pan, Nonlocal boundary layer vertical diffusion in a medium range forecast model, *Mon. Wea. Rev.*, **124**, 2322-2339, 1996.
- Jaffe, D., I. Bertschi, L. Jaegle, P. Novelli, J.S. Reid, H. Tanimoto, R. Vingarzan, and D. L. Westphal, Long-range transport of Siberian biomass burning emissions and impact on surface ozone in western North America, *Geophys. Res. Lett.*, **31**, L16106, doi:10.1029/2004GL020093, 2004.
- Kain, J. S., M. E. Baldwin, S. J. Weiss, Parameterized updraft mass flux as a predictor of convective intensity, *Wea. Forecasting*, **18**, 106-116, 2003.
- Kain, J. S., J. M. Fritsch, Convective parameterization for mesoscale models: The Kain-Fritsch scheme. *The representation of cumulus convection in numerical models*, K. A. Emanuel and D. J. Raymond, Eds., Amer. Meteor. Soc., 1993.
- Kalnay, E., M. Kanamitsu, R. Kistler, W. Collins, D. Deaven, L. Gandin, M. Iredell, S. Saha, G. White, J. Woollen, Y. Zhu, A. Leetmaa, B. Reynolds, M. Chelliah, W. Ebisuzaki, W. Higgins, J. Janowiak, K. C. Mo, C. Ropelewski, J. Wang, Roy Jenne and Dennis Joseph. 1996: The NCEP/NCAR 40-Year Reanalysis Project. *Bull. Am. Meteorol. Soc.*, **77**, No. 3, pp. 437–471
- Li, Q., D. J. Jacob, R. Park, Y. Wang, C. L. Heald, R. Hudman, R. M. Yantosca, R. V. Martin, and M. Evans, North American pollution outflow and the trapping of convectively lifted pollution by upper-level anticyclone, *J. Geophys. Res.*, **110**, D10301, doi:10.1029/2004JD005039, 2005.
- Liang, Q., L. Jaegle, D. A. Jaffe, P. Weiss-Penzias, A. Heckman, and J. A. Snow, Long-range transport of Asian pollution to the northeast Pacific: Seasonal variations and transport pathways of carbon monoxide, *J. Geophys. Res.*, **109**, D23S07, doi:10.1029/2003JD004402, 2004.

- Martin, B. D., H. E. Fuelberg, N. J. Blake, J. H. Crawford, J. A. Logan, D. R. Blake, and G. W. Sachse, Long range transport of Asian outflow to the equatorial Pacific, *J. Geophys. Res.*, **108**(D2), 8322, doi:10.1029/2001JD001418, 2003.
- Martin, J. E., The structure and evolution of a continental winter cyclone. Part II: Frontal forcing of an extreme snow event, *Mon. Wea. Rev.*, **126**, 329-348, 1988.
- Pinot, J.-M., J. Tintore, and D.-P. Wang, A study of the omega equation for diagnosing vertical motions at ocean fronts, *J. Mar. Res.*, **54**, 239-259, 1992.
- Purvis R. M., et al., Rapid uplift of nonmethane hydrocarbons in a cold front over central Europe, *J. Geophys. Res.*, **108** (D7), 4224, doi:10.1029/2002JD002521, 2003.
- Raisanen, J., Factors affecting synoptic-scale vertical motions: A statistical study using a generalized omega equation, *Mon. Wea. Rev.*, **123**, 2447-2460, 1995.
- Roebber, P. J., A statistical analysis and updated climatology of explosive cyclones, *Mon. Wea. Rev.*, **112**, 1577-1589, 1984.
- Schaer, C. and H. Wernli, Structure and evolution of an isolated semi-geostrophic cyclone. *Q. J. R. Meteorol. Soc.*, **119**, 57-90, 1993.
- Schultz, D. M., Reexamining the cold conveyor belt, *Mon. Wea. Rev.*, **129**, 2205-2225, 2001.
- Seaman, N. L., and S. A. Michelson, Mesoscale meteorological structure of a high-ozone episode during the 1995 NARSTO-Northeast study, *J. Appl. Meteor.*, **39**, 384-398, 2000.
- Singh, H. B., W. Brune, J. Crawford, and D. Jacob, Overview of the summer 2004 Intercontinental Chemical Transport Experiment-North America (INTEX-NA), *J. Geophys. Res.*, submitted.
- Stauffer, D. R., and N. L. Seaman, Use of four-dimensional data assimilation in a limited-area mesoscale model, part I, Experiments with synoptic-scale data, *Mon. Weather Rev.*, **118**, 1250-1277, 1990.
- Stauffer, D. R., and N. L. Seaman, Multiscale four-dimensional assimilation, *J. Appl. Meteorol.*, **33**, 416-434, 1994.
- Stauffer, D. R., N. L. Seaman, and F. S. Binkowski, Use of four-dimensional data assimilation in a limited area mesoscale model, part II, Effects of data assimilation within the planetary boundary layer, *Mon. Weather Rev.*, **119**, 734-754, 1991.
- Stohl, A., A one-year lagrangian "climatology" of airstreams in the northern hemisphere troposphere and lowermost stratosphere, *J. Geophys. Res.*, **106**(D7), 7263-7280, 10.1029/2000JD900570, 2001.

- Stohl, A., and P. Seibert, accuracy of trajectories as determined from the conservation of meteorological tracers, *Quart. J. Roy. Meteor. Soc.*, **124**, 1465-1484, 1998.
- Stohl, A., G. Wotawa, P. Seibert, and H. Kromp-Kolb, Interpolation errors in wind fields as a function of spatial and temporal resolution and their impact on different types of kinematic trajectories, *J. Appl. Meteor.*, **34**, 2149-2165, 1995.
- Stohl, A. and T. Trickl, A textbook example of long-range transport: Simultaneous observation of ozone maxima of stratospheric and North American origin in the free troposphere over Europe, *J. Geophys. Res.*, **104**, 30,445-30,462, 1999.
- Sutton, R., H. Maclean, R. Swinbank, A. O'Neill, and F. W. Taylor, High resolution tracer fields estimated from satellite observations using Lagrangian trajectory calculations, *J. Atmos. Sci.*, **51**, 2995-3005, 1994.
- Wakimoto, R. M., Forecasting dry microburst activity over the high plains, *Mon. Wea. Rev.*, **113**, 1131-1143, 1985.
- Warner, T. T., R. A. Peterson, and R. E. Treadon, A tutorial on lateral boundary conditions as a basic and potentially serious limitation to regional numerical weather prediction, *Bull. Am. Meteorol. Soc.*, **78**, 2599-2617, 1997.
- Wernli, H., A lagrangian-based analysis of extratropical cyclones. II: A detailed case study, *Q. J. R. Meteorol. Soc.*, **123**, 1677-1706, 1997.
- Wernli, H. and H. C. Davies, A lagrangian-based analysis of Extratropical cyclones. I: The method and some applications, *Q. J. R. Meteorol. Soc.*, **123**, 467-489, 1997.
- Young, M. V., Investigation of a cyclogenesis event, 26-29 July 1988, using satellite imagery and numerical model diagnostics, *Meteoro. Mag.*, **118**, 185-196, 1989.

Table 1. Upward mass flux (10^7 kg s^{-1}) (a) east, (b) south, and (c) southwest of the cyclones' center at four vertical levels (850, 700, 500, and 300 hPa).

a) East of Cyclone Center (Box 1)

Level (hPa)	Carlson's Case	INTEX-A Case 1
300	0	5.5
500	36.7	0.3
700	58.7	26.4
850	36.7	29.7

b) South of Cyclone Center (Box 2)

Level (hPa)	Carlson's Case	INTEX-A Case 1
300	0	38.9
500	0	59.5
700	7.3	66.4
850	48.8	97.6

c) Southwest of Cyclone Center (Box 3)

Level (hPa)	Carlson's Case	INTEX-A Case 1
300	0	8.8
500	0	25.3
700	0	47.7
850	34.9	61.3

Table 2. Convective upward mass flux (CMF) (10^7 kg s^{-1}) south and southwest of the center of the INTEX-A case 1 cyclone at four vertical levels (850, 700, 500, and 300 hPa). Since values are zero east of the cyclone (Box 1), they are not listed here.

Level (hPa)	South of Cyclone (Box 2)	Southwest of Cyclone (Box 3)
300	53.1	6.8
500	42.3	35.7
700	38.4	51.1
850	0	40.2

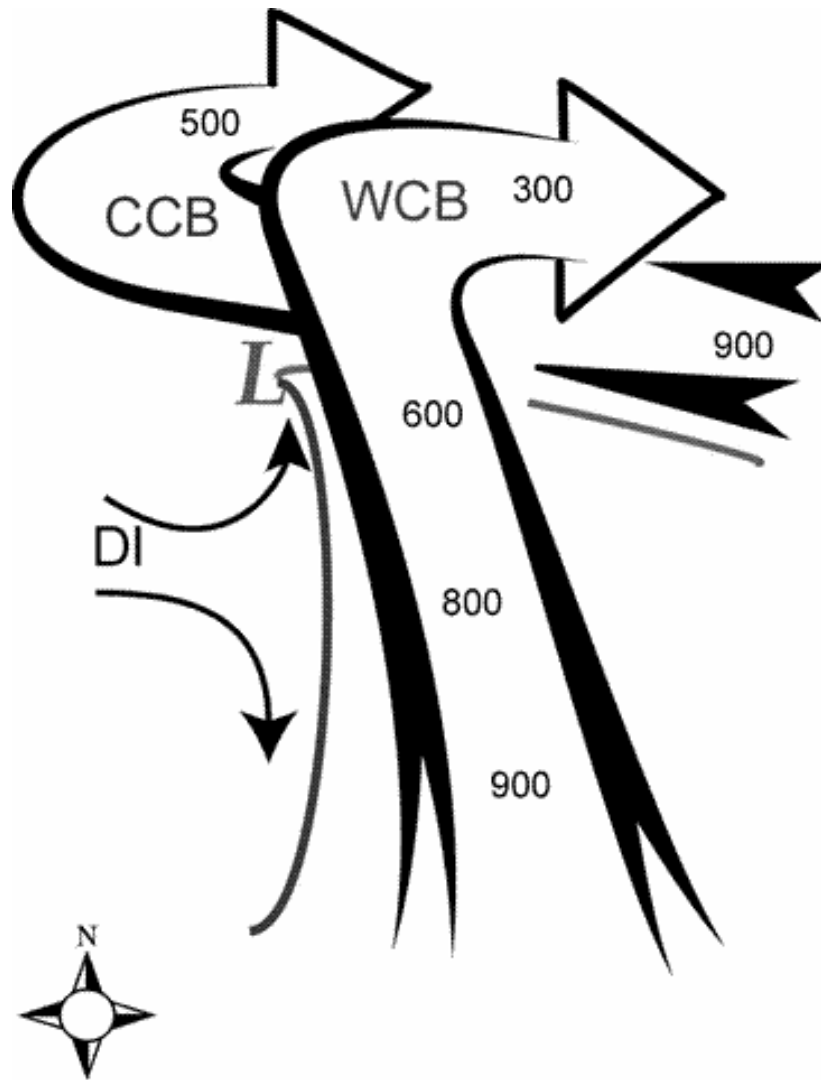
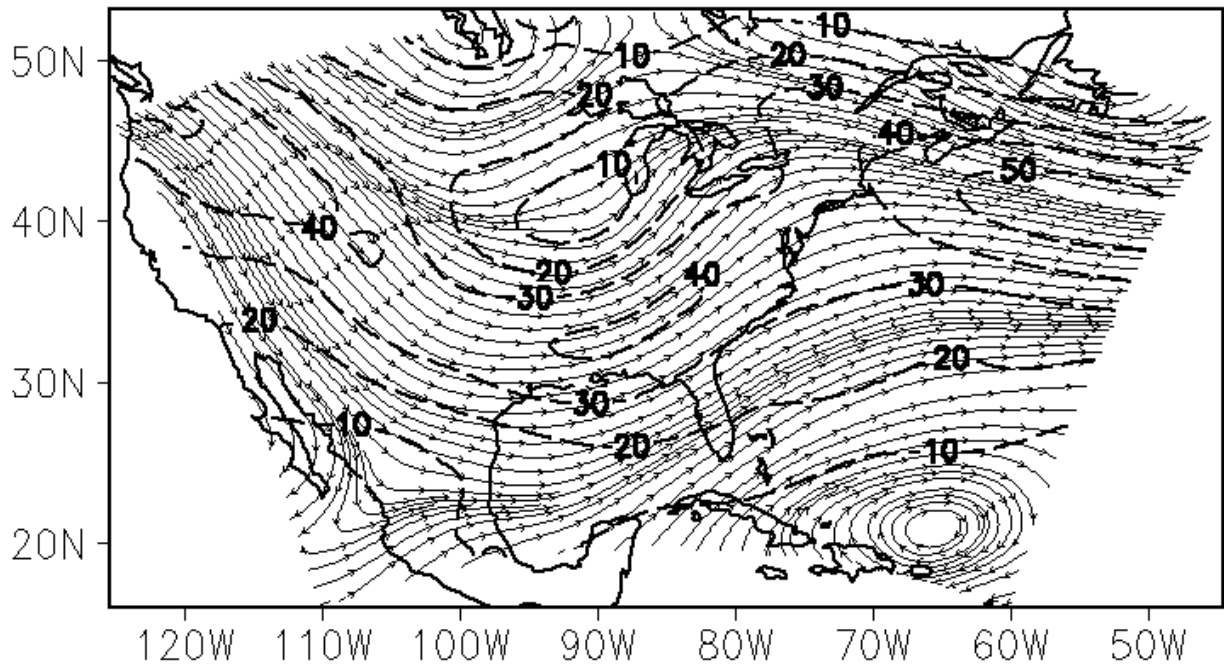


Figure 1. Airstream configuration as depicted in the classic cyclone model (adapted from *Carlson, 1980*). Airstreams are the warm conveyor belt (WCB), cold conveyor belt (CCB), and dry intrusion (DI). Numbers indicate the approximate pressure altitudes (hPa) of the airstreams. The surface low-pressure center is indicated with an “L”. The lines extending south and east of the low-pressure center indicate the surface cold front and warm front, respectively.

a)

500 hPa Steamlines and Isotachs (m s^{-1})



b)

Sea Level Pressure

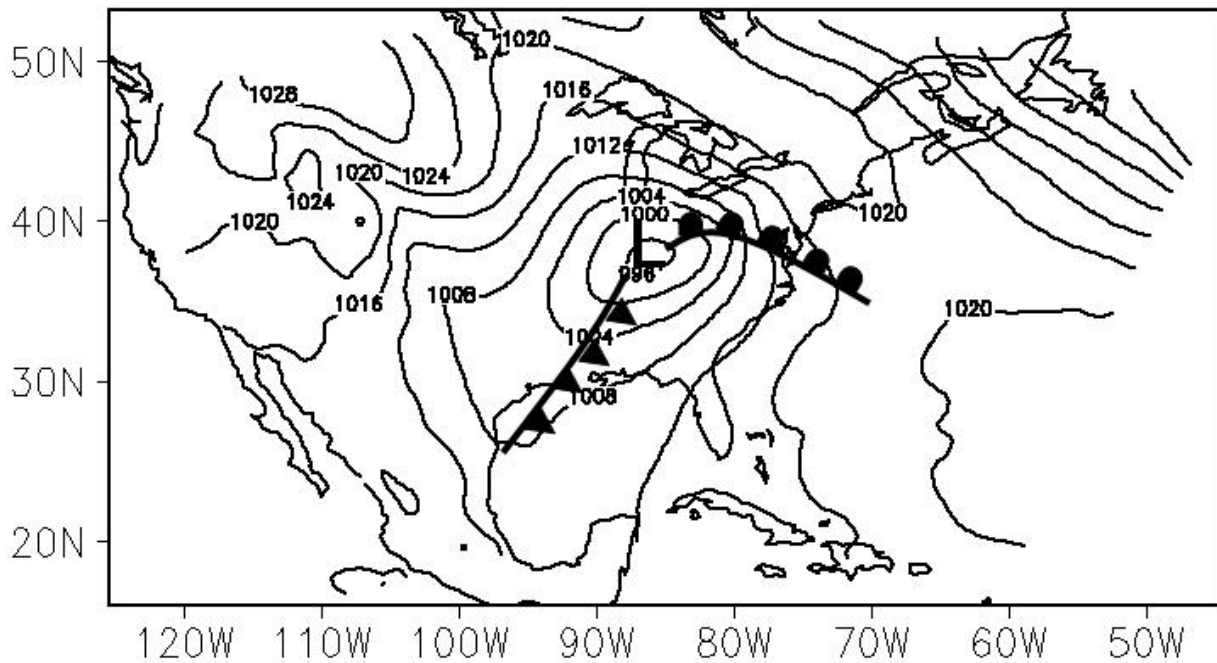


Figure 2. MM5 48 h forecast valid at 1200 UTC 5 December 1977, time of the cyclone's maximum intensity. (a) Sea level pressure (hPa), (b) 500 hPa streamlines and isotachs (m/s).

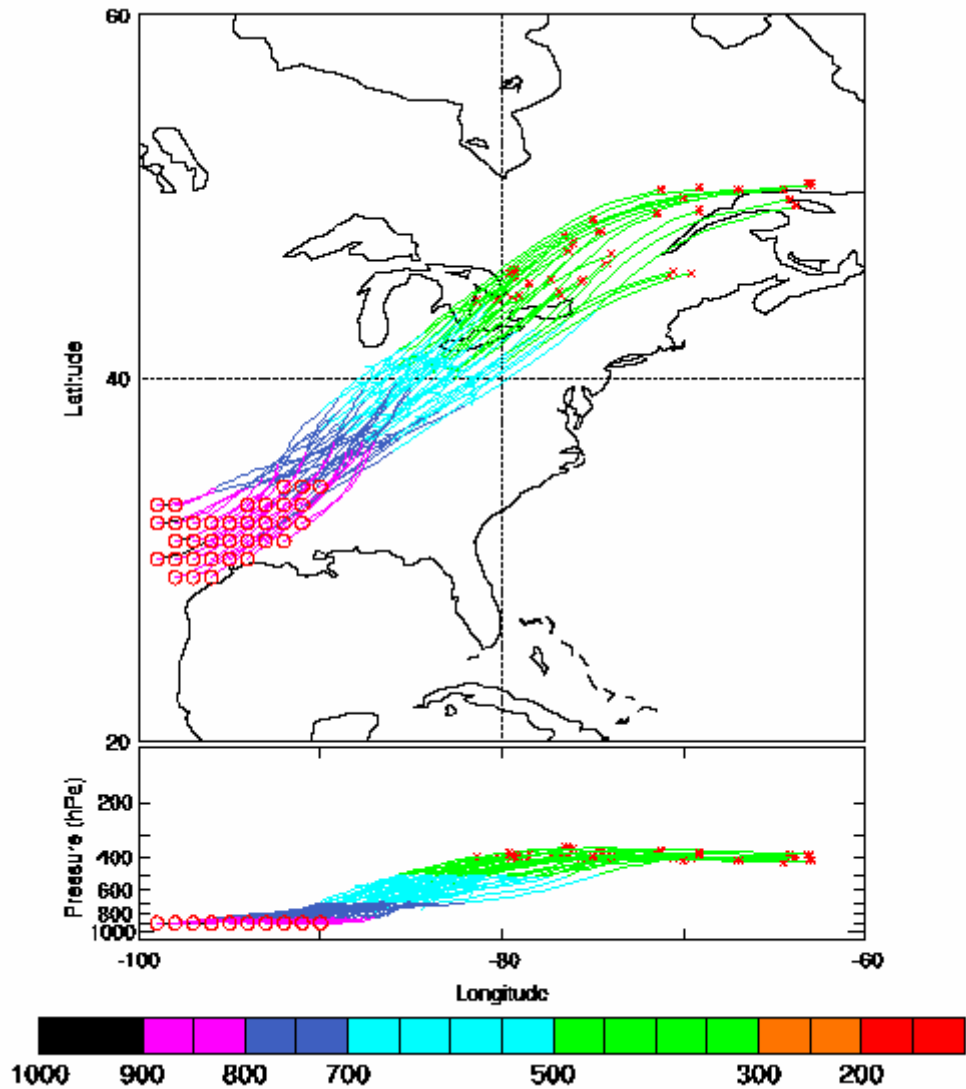


Figure 3. 48 h coherent ensemble of forward trajectories started at 1200 UTC 4 December 1977. The top panel shows a horizontal perspective of the CET trajectories, while the lower panel provides their pressure altitude vs. longitude. The color scheme indicates trajectory altitude. An “x” at the end of the trajectory indicates that the parcel has exited the data domain before completing the 48 h period. Conversely, an asterisk “*” indicates that the trajectory has completed the 48 h period inside the data domain.

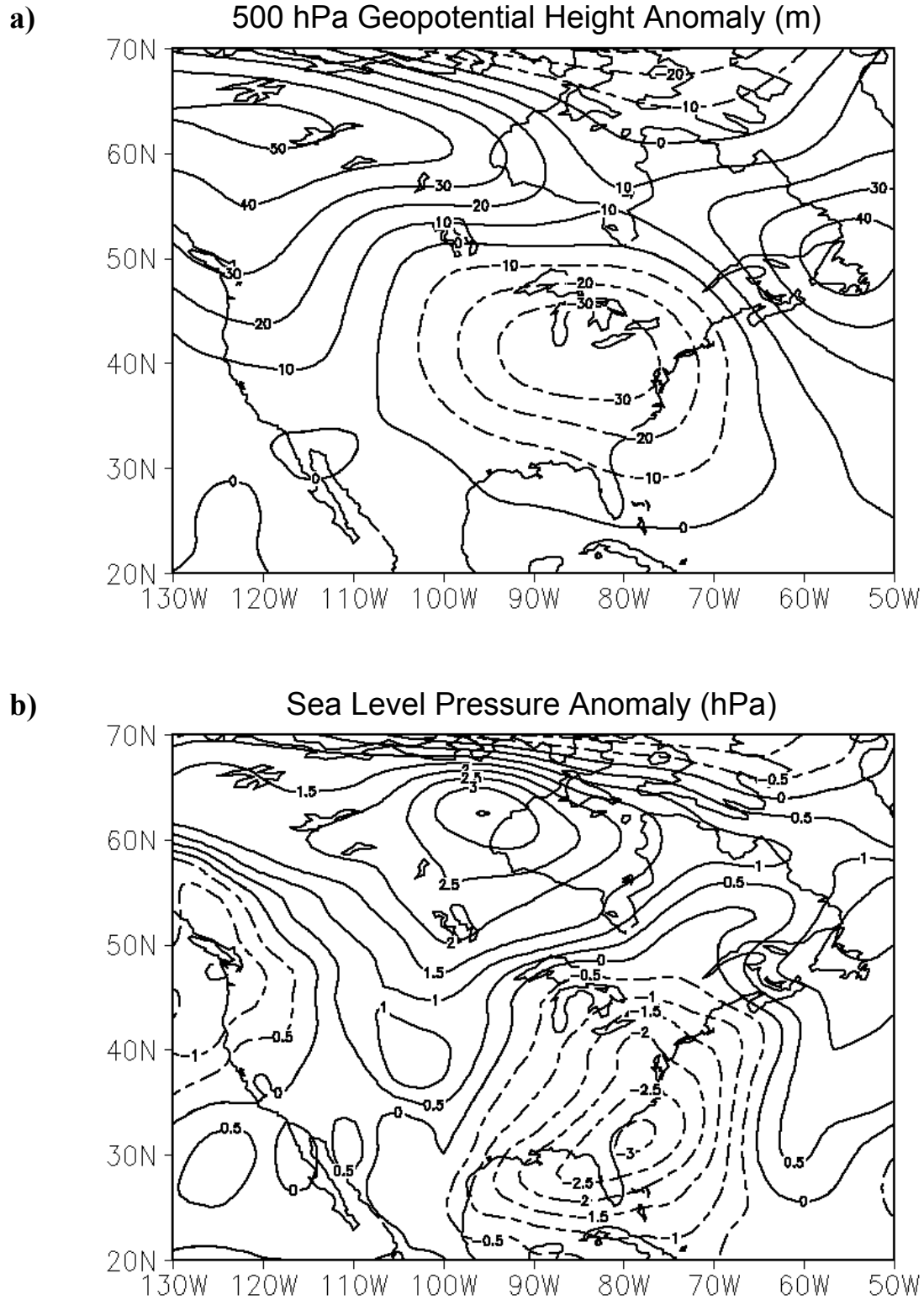
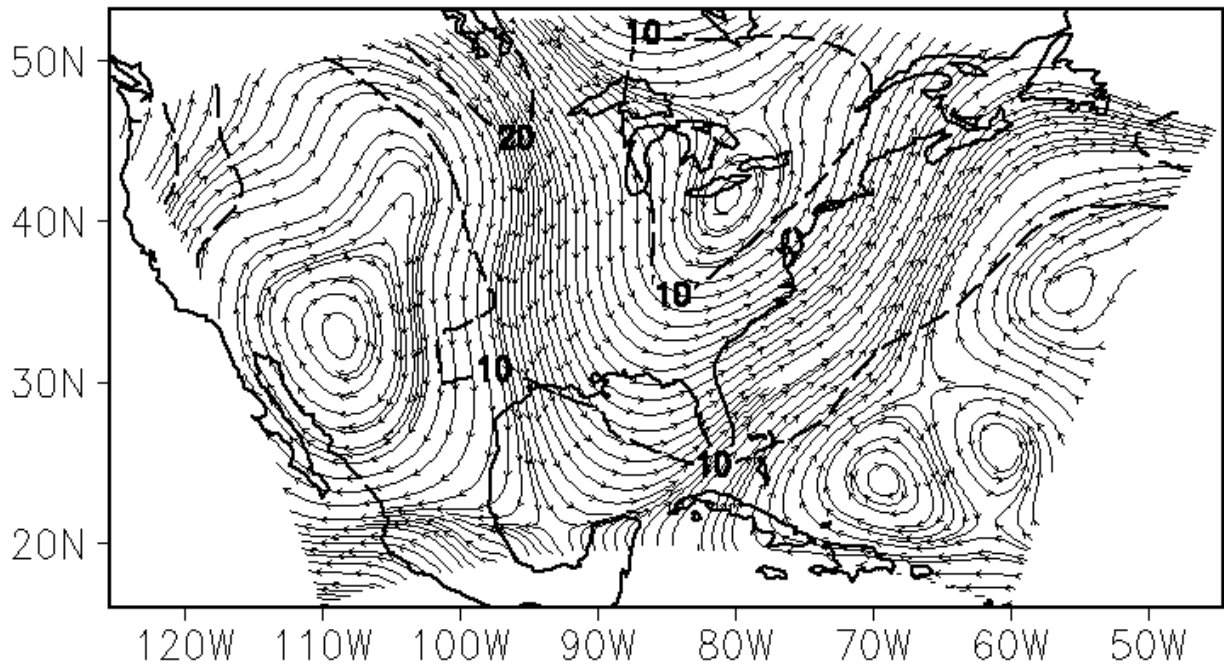


Figure 4. Anomaly (1979-1995) of (a) 500 hPa geopotential height (m) and (b) sea level pressure (hPa) for the 7 week INTEX-A period, 1 July – 15 August 2004.

a)

500 hPa Steamlines and Isotachs (m s^{-1})



b)

Sea Level Pressure

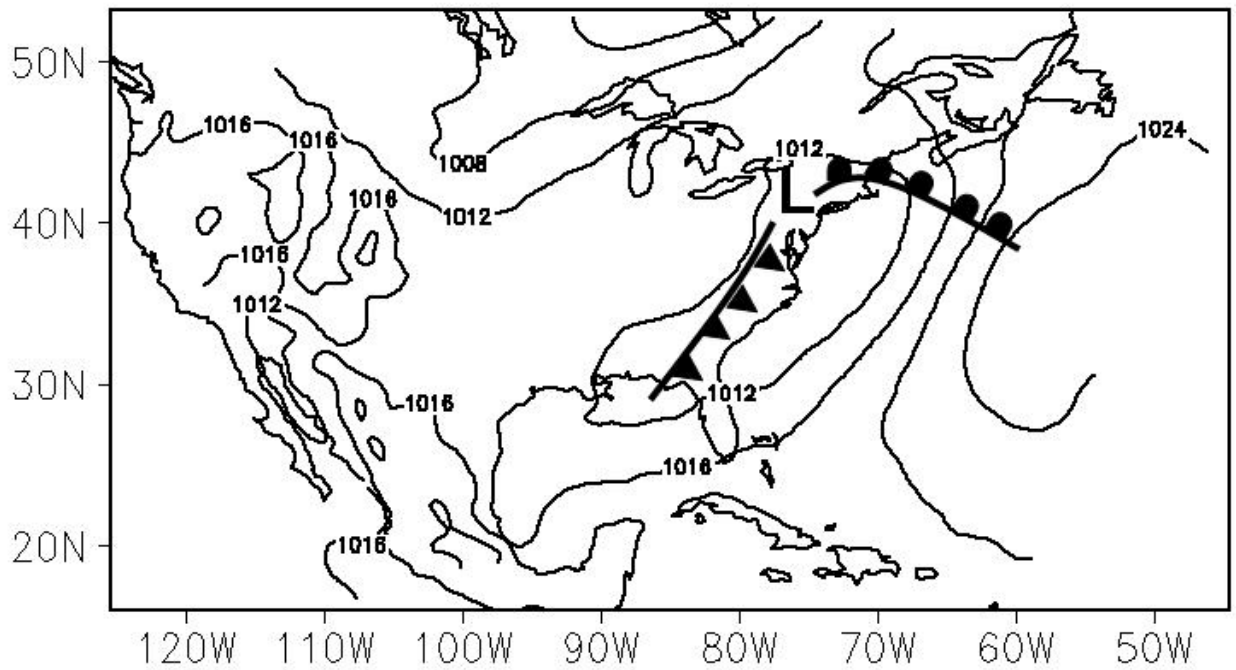


Figure 5. MM5 48 h forecast valid at 0600 UTC 19 July 2004, time of the cyclone's maximum intensity. (a) 500 hPa streamlines and isotachs (m s^{-1}), (b) Sea level pressure.

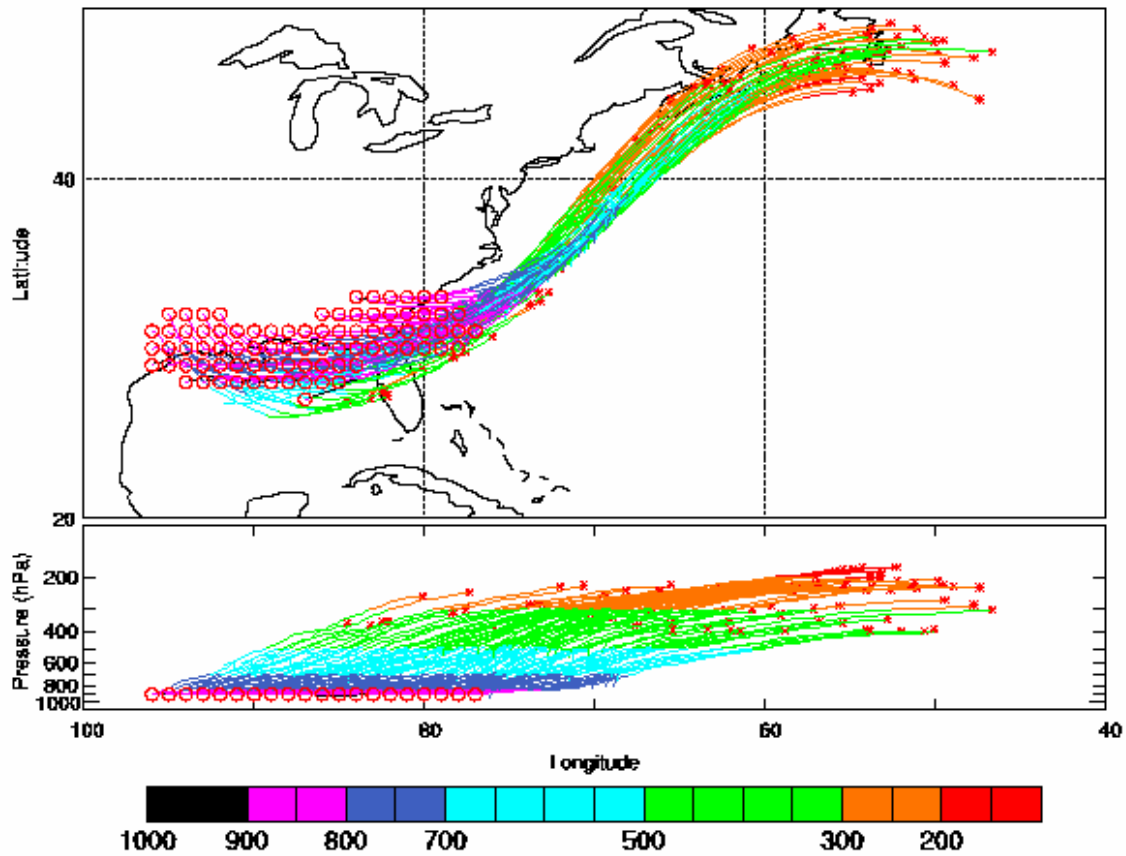
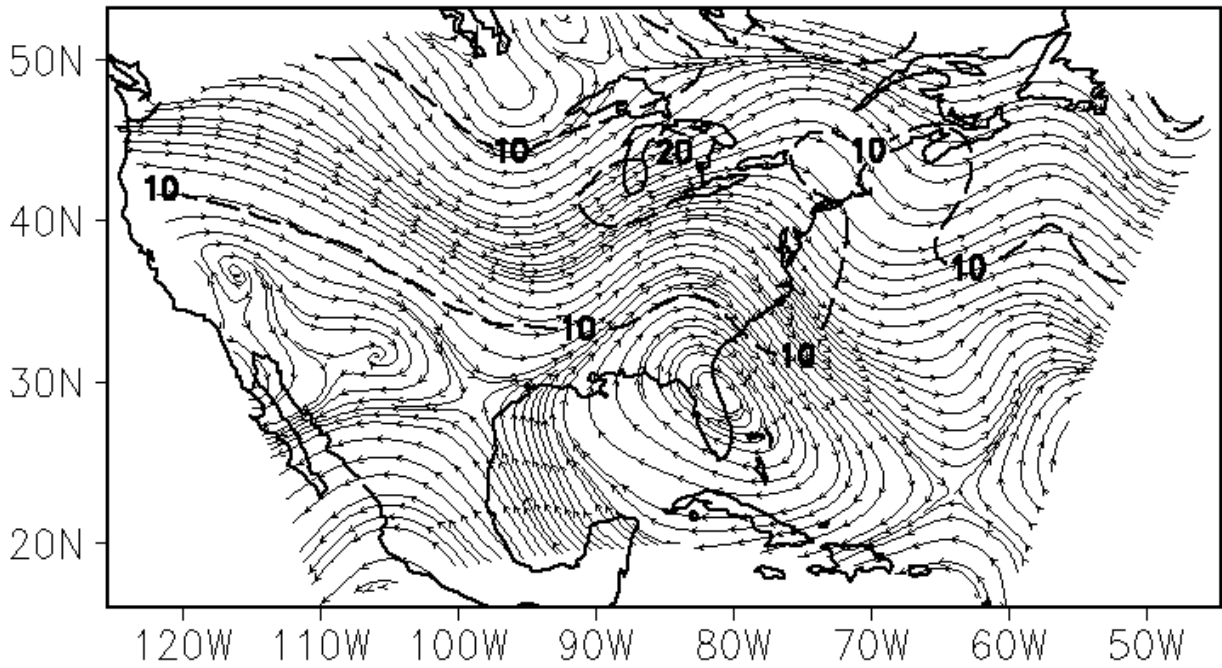


Figure 6. 48 h coherent ensemble of forward trajectories started at 0600 UTC 19 July 2004. The top panel shows a horizontal perspective of the CET trajectories, while the lower panel provides their pressure altitude vs. longitude. The color scheme indicates trajectory altitude. An “x” at the end of the trajectory indicates that the parcel has exited the data domain before completing the 48 h period. Conversely, an asterisk “*” indicates that the trajectory has completed the 48 h period inside the data domain.

a) 500 hPa Steamlines and Isotachs (m s^{-1})



b) Sea Level Pressure

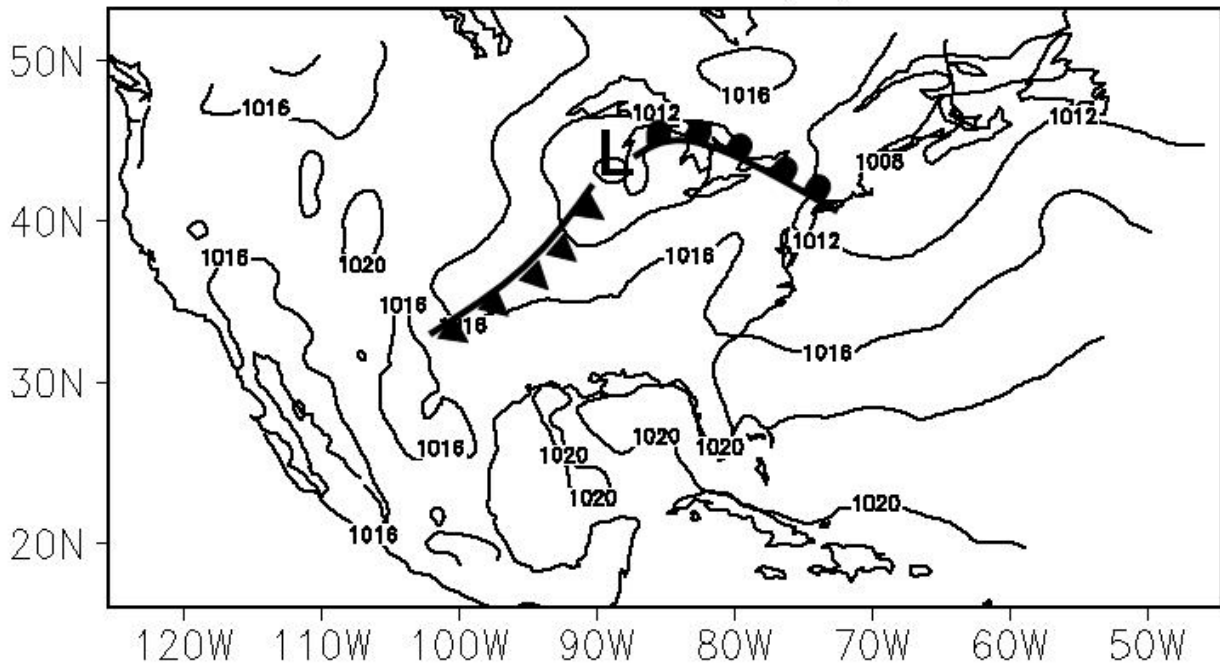
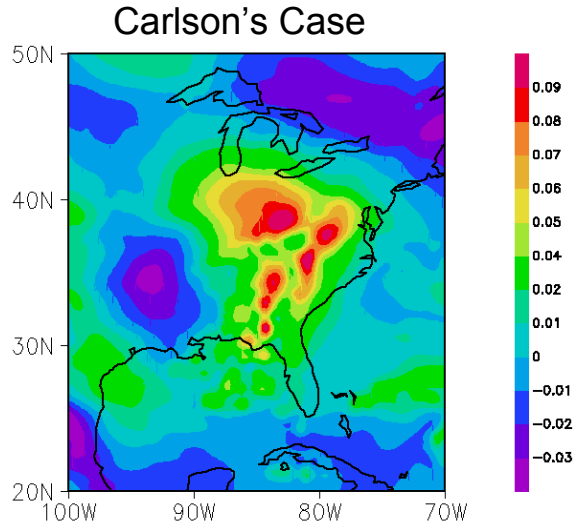
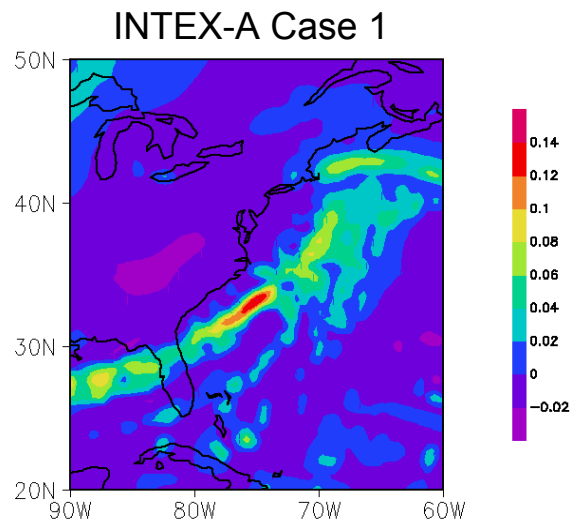


Figure 7. MM5 48 h forecast valid at 1800 UTC 6 July 2004, time of the cyclone's maximum intensity. (a) 500 hPa streamlines and isotachs (m s^{-1}), (b) Sea level pressure (hPa).

a)



b)



c)

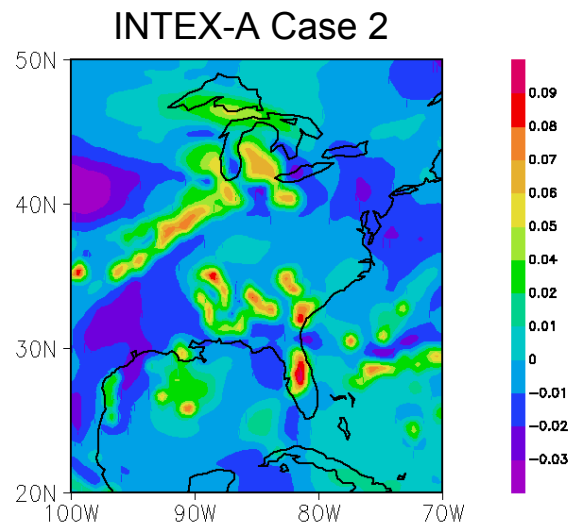


Figure 8. MM5 48 h forecast 700 hPa vertical motion (m s^{-1}) for (a) Carlson's case, (b) INTEX-A case 1, and (c) INTEX-A case 2. Please note the different scale used in (b).

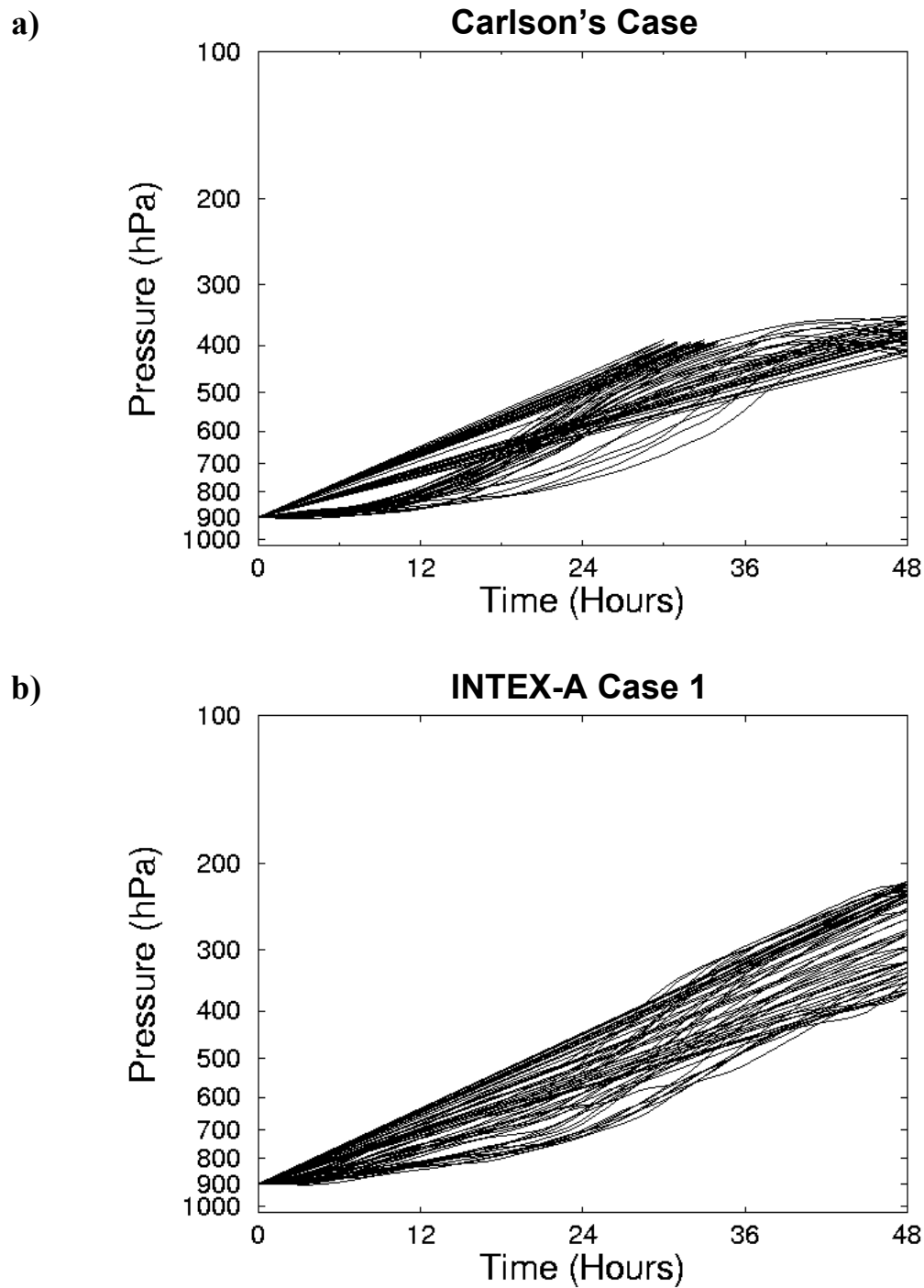
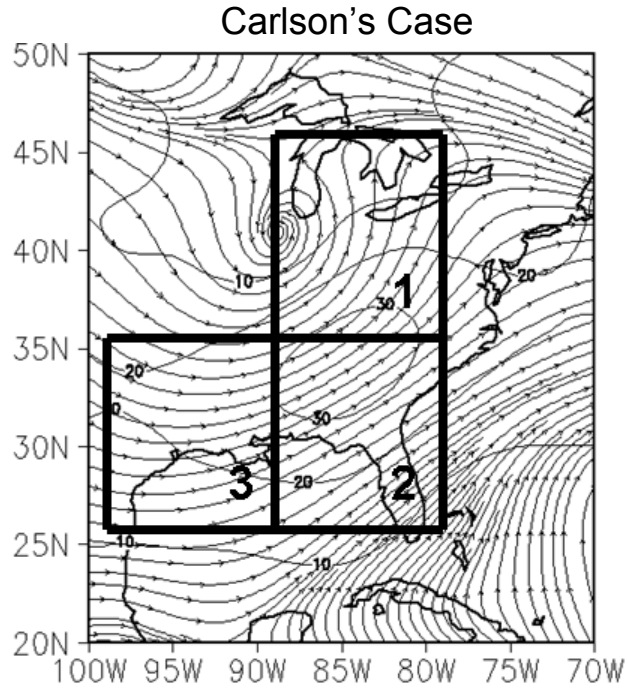


Figure 9. Plot of 48 h trajectory heights (hPa) vs. time (h) for (a) Carlson's case and (b) INTEX-A case 1. All trajectories starting at 900 hPa and meeting the criteria are shown. Some trajectories leave the domain before the end of the 48 h period.

a)



b)

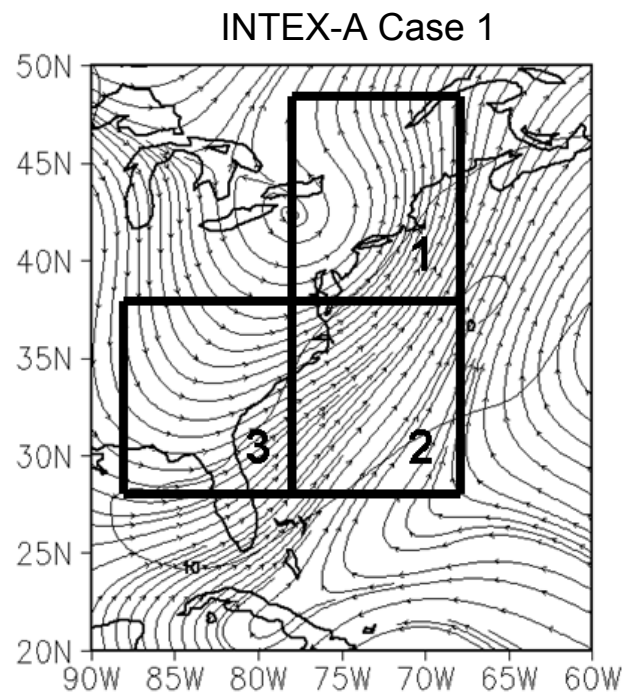


Figure 10. MM5 forecast of 700 hPa streamlines at the time of maximum cyclone intensity with the three $10^\circ \times 10^\circ$ study areas for each cyclone superimposed (see text for details). (a) Carlson's case (1200 UTC 5 December 1977), (b) INTEX-A case 1 (0600 UTC 19 July 2004).

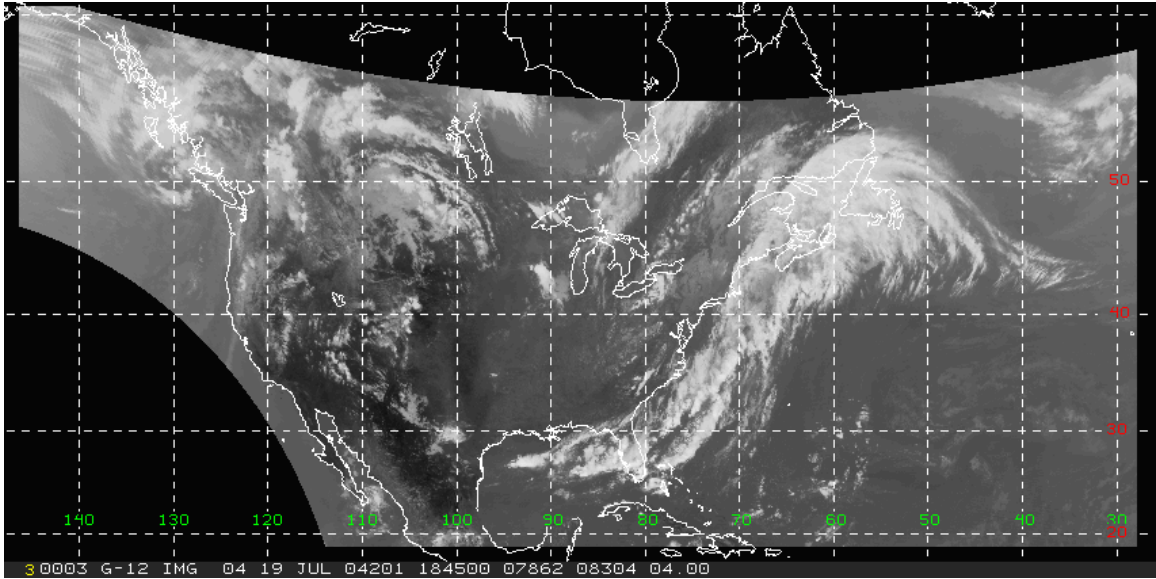


Figure 11. Infrared image from Geostationary Operational Environmental Satellite (GOES) 12 at 1845 UTC 19 July 2004.

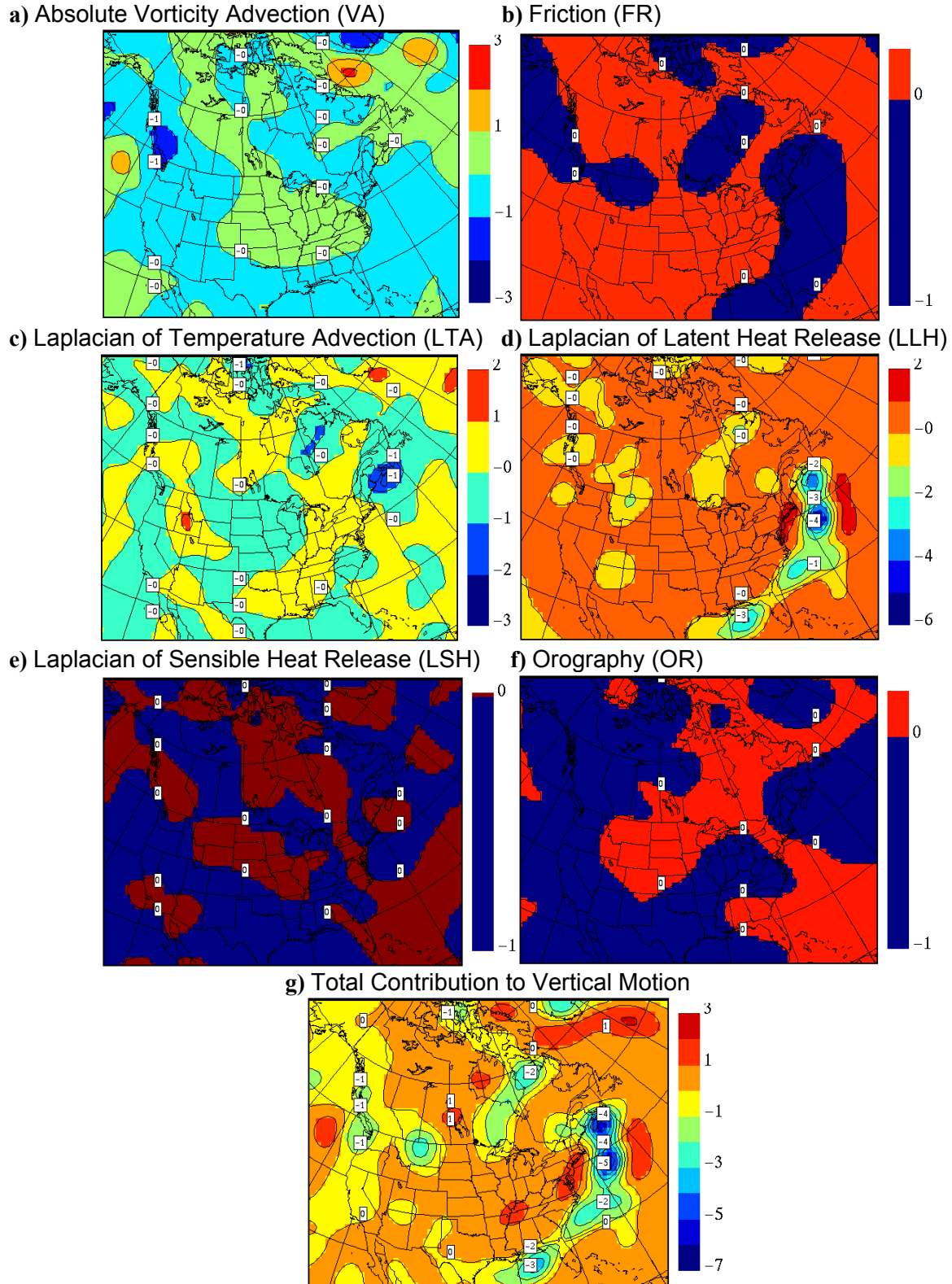
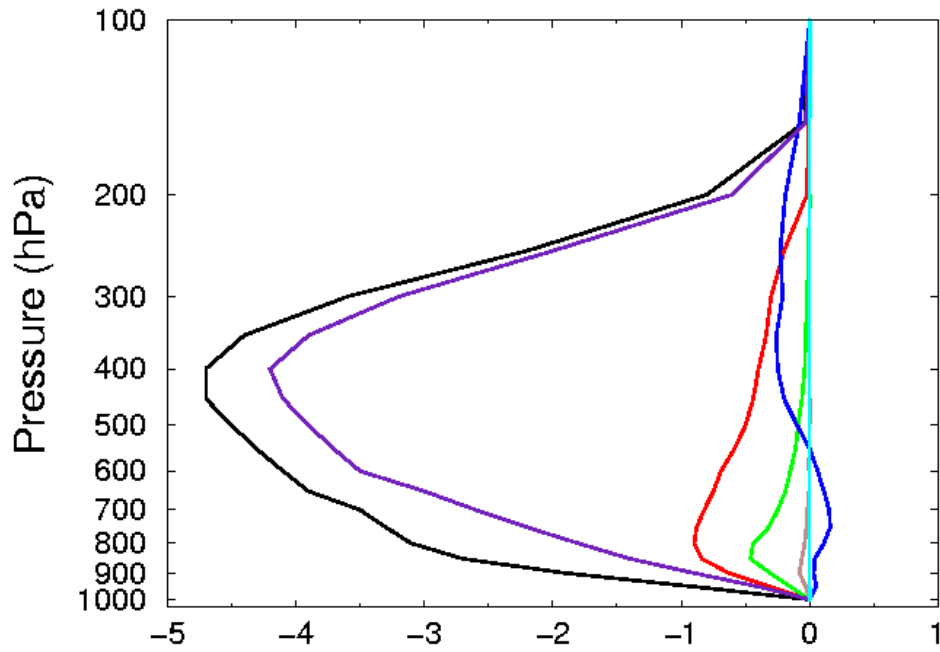


Figure 12. Contribution of forcing terms to vertical motion ($10^{-1} \text{ Pa s}^{-1}$) at 500 hPa for INTEX-A case 1, 0600 UTC 19 July 2004.

a) Contribution of Forcing Terms to Vertical Motion ($10^{-1} \text{ Pa s}^{-1}$)
 VA (red) FR (green) LTA (blue) LLH (purple) LSH (brown) OR (cyan) TOT (black)



b) Contribution of Forcing Terms to Vertical Motion ($10^{-1} \text{ Pa s}^{-1}$)
 VA (red) FR (green) LTA (blue) LLH (purple) LSH (brown) OR (cyan) TOT (black)

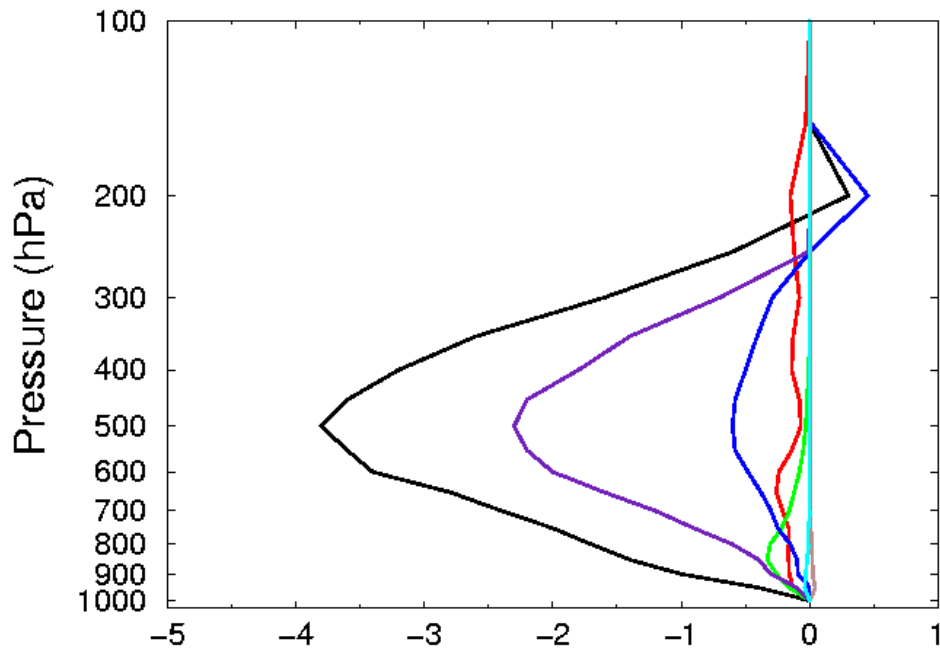


Figure 13. Vertical profile of the contribution of various forcing terms to vertical motion ($10^{-1} \text{ Pa s}^{-1}$) for INTEX-A Case 1, 0600 UTC 19 July 2004 at (a) 38° N , 68° W and (b) 28° N , 86° W .

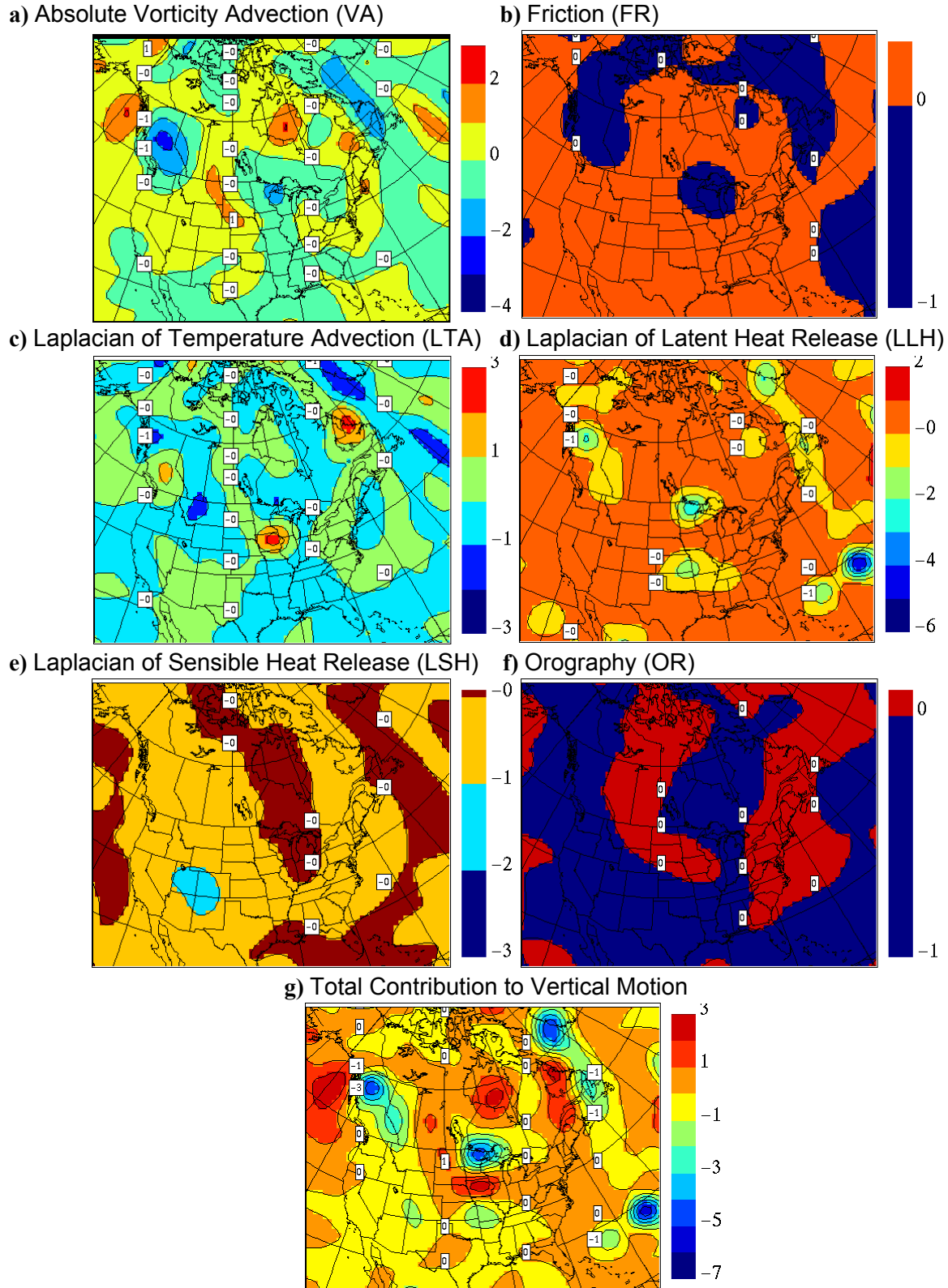


Figure 14. Contribution of forcing terms to vertical motion ($10^{-1} \text{ Pa s}^{-1}$) at 500 hPa for INTEX-A Case 2, 1800 UTC 6 July 2004.

Contribution of Forcing Terms to Vertical Motion ($10^{-1} \text{ Pa s}^{-1}$)
VA (red) FR (green) LTA (blue) LLH (purple) LSH (brown) OR (cyan) TOT (black)

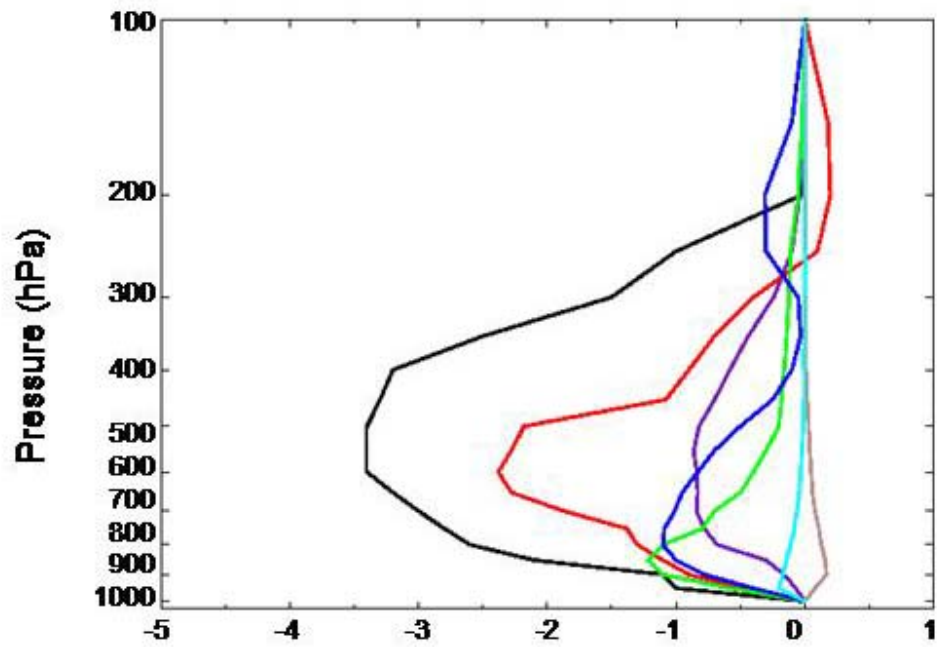


Figure 15. Vertical profile of the contribution of forcing terms to vertical motion ($10^{-1} \text{ Pa s}^{-1}$) for INTEX-A Case 2, 1800 UTC 6 July 2004 at 49° N , 96° W .

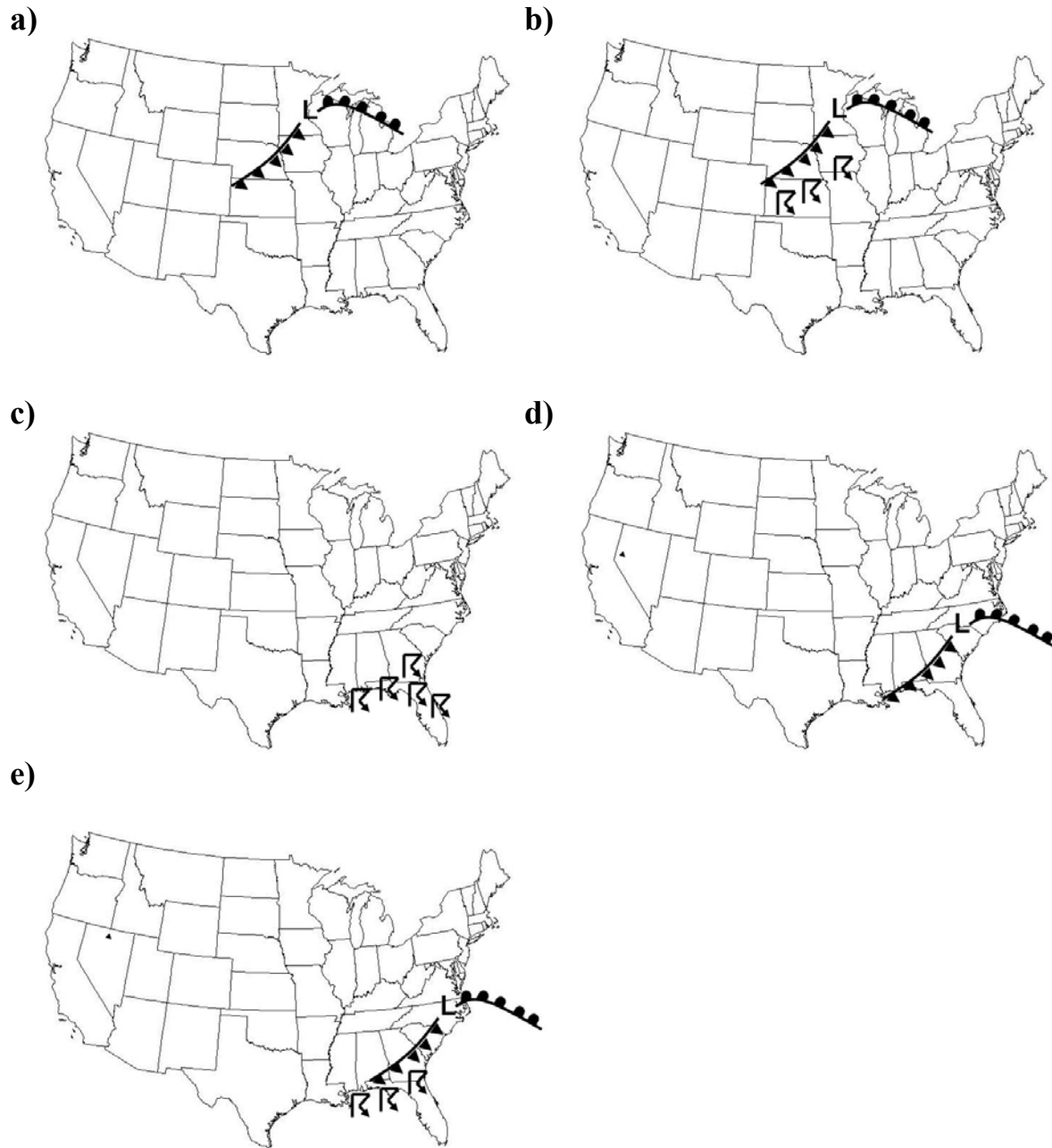


Figure 16. Five generalized warm season synoptic patterns (see text for details). (a) Front north of Gulf Coast with no widespread convection, (b) Front north of Gulf Coast with widespread convection, (c) Gulf Coast convection with no front, (d) Gulf Coast front with no widespread convection, (e) Gulf Coast front with widespread convection.